

Dynamical R-parity Breaking at the LHC

Shao-Long Chen,^{a,b} Dilip Kumar Ghosh,^c Rabindra N. Mohapatra,^a Yue Zhang^d

^a*Maryland Center for Fundamental Physics and Department of Physics,
University of Maryland, College Park, Maryland 20742, USA*

^b*Institute of Particle Physics, Huazhong Normal University, Wuhan 430079, China*

^c*Department of Theoretical Physics, Indian Association for the Cultivation of Science,
2A&2B Raja S.C. Mullick Road, Kolkata 700 032, India*

^d*Abdus Salam International Centre for Theoretical Physics, Strada Costiera 11, I-34014 Trieste, Italy*

E-mail: chensl@iopp.cnu.edu.cn, dilipghoshjal@gmail.com,
rmohapat@umd.edu, yuezhang@ictp.it

ABSTRACT: In a class of extensions of the minimal supersymmetric standard model with (B-L)/left-right symmetry that explains the neutrino masses, breaking R-parity symmetry is an essential and dynamical requirement for successful gauge symmetry breaking. Two consequences of these models are: (i) a new kind of R-parity breaking interaction that protects proton stability but adds new contributions to neutrinoless double beta decay and (ii) an upper bound on the extra gauge and parity symmetry breaking scale which is within the large hadron collider (LHC) energy range. We point out that an important prediction of such theories is a potentially large mixing between the right-handed charged lepton (e^c) and the superpartner of the right-handed gauge boson (\widetilde{W}_R^+), which leads to a brand new class of R-parity violating interactions of type $\widetilde{\mu}^c \nu_\mu^c e^c$ and $\widetilde{d}^c u^c e^c$. We analyze the relevant constraints on the sparticle mass spectrum and the LHC signatures for the case with smuon/stau NLSP and gravitino LSP. We note the “smoking gun” signals for such models to be lepton flavor/number violating processes: $pp \rightarrow \mu^\pm \mu^\pm e^+ e^- jj$ (or $\tau^\pm \tau^\pm e^+ e^- jj$) and $pp \rightarrow \mu^\pm e^\pm b\bar{b}jj$ (or $\tau^\pm e^\pm b\bar{b}jj$) without significant missing energy. The predicted multi-lepton final states and the flavor structure make the model be distinguishable even in the early running of the LHC.

ARXIV EPRINT: [1011.2214](https://arxiv.org/abs/1011.2214)

Contents

1	Introduction	1
2	Spontaneous R-parity Violation with Extended Gauge Symmetry	4
3	An Explicit Model of Dynamical R-parity Breaking	6
3.1	SUSYLR: No gauge symmetry breaking without R-parity breaking	6
3.2	Neutrino mass and flavor alignment of R-parity violation	9
4	Single Production of Slepton NLSP and its Decay at the LHC	11
4.1	Relevant RPV couplings	11
4.2	Branching ratios of slepton NLSP decay	12
4.3	$pp \rightarrow e^+e^-\mu^\pm\mu^\pm jj$	15
4.4	$pp \rightarrow \mu^\pm e^\pm b\bar{b}jj$	20
5	Some Generic Low-energy Constraints	23
5.1	Neutrinoless double beta decay	23
5.2	$\pi^0 \rightarrow e^+e^-$ decay	24
6	Conclusion	24
A	Fully parity symmetric version	25
B	Explicit form of charged fermion mass matrix	26

1 Introduction

Supersymmetry (SUSY) is one of the popular and best motivated candidates for physics beyond the standard model (SM). It stabilizes the gauge hierarchy and provides a dark matter candidate in a natural manner. An intuitive requirement to stabilize the dark matter in MSSM is the existence of the R-parity symmetry under which all standard model particles are even and their superpartners are odd. The lightest supersymmetric partner field (LSP), e.g., either the neutralino or the gravitino, which is odd under R-parity is therefore suitable as the dark matter candidate. If R-parity is a global symmetry of the MSSM, it is logical to think of it as a remnant of some high scale physics. It will of course be interesting if the high scale physics is motivated by further reasons. A shortcoming of R-parity conserving MSSM is the zero neutrino mass. Understanding the origin neutrino masses then requires it to be part of a larger theory. An example of extension to the MSSM is to gauge the $B - L$

global symmetry, where anomaly freedom requires introducing a right-handed neutrino to each generation. The breaking of $B - L$ symmetry gives Majorana masses to neutrinos. If the breaking is accomplished by Higgs fields with $B - L = \pm 2$, it not only helps to explain the small neutrino masses via the seesaw mechanism, but also leaves the R-parity as an unbroken symmetry at the level of the MSSM [1], thereby providing a stable dark matter candidate. Extending MSSM by a $B - L$ symmetry therefore “kills two birds with one stone”.

Two possible classes of models with $B - L$ gauge symmetry are: (i) $SU(2)_L \times U(1)_Y \times U(1)_{B-L}$, and (ii) its left-right (LR) symmetric generalization based on $SU(2)_L \times SU(2)_R \times U(1)_{B-L}$. Breaking $B - L$ by two units in the second case is more appealing since it can explain the origin parity violation, and leads to a number of interesting phenomenological implications for LHC searches including the W_R boson as well for low energy weak processes. We discuss them in this paper.

If the gauge symmetry is to be broken by a pair of Higgs superfields $\Delta^c(1, 3, +2) \oplus \bar{\Delta}^c(1, 3, -2)$ which are required to implement the seesaw mechanism and gauge anomaly cancellation, two interesting results follow [2]. First, even though a priori the model is expected to have a remnant R-parity after symmetry breaking, in its minimal version, exactly the opposite happens, i.e., R-parity must be necessarily broken spontaneously in order for the full gauge symmetry to break down to the MSSM gauge group. If R-parity is exact, gauge symmetry cannot break [2]. If the model is extended to include singlets, there is a range of parameters where one can still have unbroken R-parity [3]. In the minimal model, however, R-parity breaking is mandatory. The right-handed (RH) sneutrino field, $\tilde{\nu}^c$, has to pick up a vacuum expectation value (VEV) along with the neutral member of the $B - L = 2$ triplet, breaking the parity symmetry and contributing to the mass of the gauge bosons and gauginos associated with right-handed currents. Since $\tilde{\nu}^c$ is an R-odd particle, its VEV breaks R-parity. We call this class of models “dynamical R-parity breaking” models, since R-parity breaking is forced on the theory at the global minimum of the Hamiltonian. Other examples of models where R-parity breaking by ν^c vev are the minimal $U(1)_{B-L}$ extensions of the MSSM [4, 5]. In this note we will focus on the SUSYLR case.

A consequence of dynamical R-parity breaking in minimal SUSYLR model is the prediction of an upper bound on the mass scale of the right-handed W_R boson, i.e., $M_{W_R} \lesssim M_{\text{SUSY}}/f^2$ [6], which is in the range accessible at the LHC. Here M_{SUSY} is a generic soft SUSY breaking mass scale, f is the Yukawa coupling responsible for right-handed neutrino masses and has to be $\gtrsim 0.1$. Similar relations are also found in SUSYLR models where $\tilde{\nu}^c$ vevs break left-right symmetry [7, 8].

Due to spontaneous R-parity breaking, neutrino masses arise not only from the usual type-I seesaw mechanism, but also via mixing with the neutralinos. Another consequence is that neutralino is no longer a stable particle and cannot therefore play the role of dark matter. However, if gravitino is the LSP, it can have an extremely long lifetime ($\geq 10^{26}$ sec) and play the role of dark matter [9]. Implications for such a dark matter particle have been studied extensively in connection with cosmic ray anomalies [10].

Since the scales of both superpartners and the new gauge interactions are predicted to lie

in the few TeV range, this theory could in principle be testable at the hadron colliders [11]. In this paper therefore, we study the genuine signals from dynamical R-parity breaking and discuss how it can be distinguished from usual R-parity breaking models at LHC.

We point out that the most important consequence of dynamical R-parity breaking in SUSYLR models is a *large* mixing between the RH charged lepton and RH wino, i.e., the physical RH charged lepton after symmetry breaking is generically denoted as

$$\hat{\ell}^c = \theta_{\ell\ell}\ell^c + \theta_{\ell W}\widetilde{W}_R^+ + \dots, \quad (1.1)$$

where $\theta_{\ell\ell}, \theta_{\ell W} \sim \mathcal{O}(1)$ for $\langle \tilde{\nu}^c \rangle \simeq M_{\text{SUSY}}$ and the \dots represents the contributions of other Higgsino fields if the corresponding Higgses VEV's also violate parity. The physical charged lepton field contains a large RH wino component and in turn induces new R-parity violating terms of Kähler type. This is characteristic of dynamical R-parity breaking models [2, 7, 8] with the presence of gauged $SU(2)_R$ and it leads to new effects absent in usual R-parity violating MSSM or other models of spontaneous R-parity breaking, such as [12, 13]. In particular, it leads to effective R-parity violating interactions of the form $\tilde{\mu}^{c\dagger}\nu_\mu^c e^c$, $\tilde{\tau}^{c\dagger}\nu_\tau^c e^c$ and $\tilde{d}^{c\dagger}u^c e^c$ for all generations of quarks/squarks. We show that these kinds of vertices add new contributions to neutrinoless double beta decay and imply constraints on the parameters of the model.

These new interactions bring rich phenomenology at the LHC. In the context of a realistic model based on left-right symmetry, we study the single production of a slepton NLSP from the RH neutrino decays, which is produced via an on-shell W_R boson resonance at LHC. The NLSP single production and decay yield multi-lepton final states of type $pp \rightarrow \mu^\pm\mu^\pm e^+e^-jj$ (or $\tau^\pm\tau^\pm e^+e^-jj$) and $pp \rightarrow \mu^\pm e^\pm b\bar{b}jj$ (or $pp \rightarrow \tau^\pm e^\pm b\bar{b}jj$) which break both lepton number and flavor and have no missing energy. The parent states could therefore be reconstructed up to the original W_R decay. The lepton final states are predicted to have distinct flavor structures. We further point out that the $\ell^c - \widetilde{W}_R^+$ mixing also leads to the production of righthanded polarized top quarks from down-type squark decay, which is distinguishable from the $\lambda'QLd^c$ trilinear couplings in the usual R-parity violating MSSM [14].

In section II, we study the general features in a class of models where R-parity is broken together with extra gauge symmetries. We derive new R-parity breaking terms from the Kähler potential and point out how to distinguish this class of model from others, e.g. the MSSM with usual R-parity breaking terms. In section III, we review the symmetry breaking in the context of minimal supersymmetric left-right (SUSYLR) model, emphasizing the necessity of spontaneous (dynamical) R-parity violation for $SU(2)_R$ gauge symmetry breaking. We discuss the flavor issues of R-parity breaking and its implications to neutrino mass and in section IV, we study the signatures of the model at the LHC. We mainly focus on the single production and decay of slepton NLSP via a heavier RH neutrino. The predicted multi-lepton final states and the flavor structure make the model distinguishable even in the early running of the LHC. Finally in section V, we point out a new contribution to the neutrinoless double beta decay in the model and conclude.

2 Spontaneous R-parity Violation with Extended Gauge Symmetry

Unlike explicit R-parity violation, spontaneous R-parity violation (SRPV) has the advantage that it introduces only one new parameter into the R-parity conserving theory – the VEV of an R-parity-odd field. Furthermore, if R-parity violating scale is at the TeV range, above this temperature, R-parity is exact and therefore it is less constrained by cosmology.

SRPV can be realized in various ways: in the first model where the idea was discussed [12], the superpartner of SM neutrino was given a non-zero VEV. Since lepton number is not a gauge symmetry of the MSSM, this leads to a doublet majoron which contributes to the Z -boson width and LEP measurements therefore have ruled out this scenario. One could of course implement SRPV by the VEV of a right-handed sneutrino [13] in extensions of the MSSM that explain neutrino masses. Since the right-handed sneutrino field is a standard model singlet, the majoron does not couple to the Z -boson and therefore escapes the constraints set by the LEP data.

In this section, we will pursue the implications when the R-parity is spontaneously broken together with some extra gauge symmetry beyond $\mathbf{G}_{SM} = SU(2)_L \times U(1)_Y$. Here we focus on the class of models where the extended gauge group \mathbf{G} contains a subgroup $SU(2)_R$. Clearly, the RH neutrino and its superpartner will be charged under the $SU(2)_R$. Giving a non-zero VEV to $\tilde{\nu}^c$ will therefore give rise to new interactions. Models with dynamical R-parity breaking belong to this category. Furthermore, such model predicts that the scale of new gauge interactions is tied to the soft SUSY breaking scale. This leads to several interesting new features as we show below.

The key distinguishing prediction of such a model is the existence of a large mixing between RH charged leptons and the gaugino superpartner of the W_R boson. Since we work with the gauge group $\mathbf{G} = SU(2)_L \times SU(2)_R \times U(1)_{B-L}$, the RH neutrino and charged lepton form a doublet under $SU(2)_R$.

After the RH sneutrino developing a VEV

$$\langle \tilde{L}^c \rangle = \begin{bmatrix} \langle \tilde{\nu}^c \rangle \\ 0 \end{bmatrix}, \quad (2.1)$$

it breaks both the $SU(2)_R$ gauge group as well as the R-parity, at the scale of $\langle \tilde{\nu}^c \rangle$. Due to the Higgs mechanism, the heavy gauge bosons acquire their mass by absorbing the scalars $\mathcal{I}m \tilde{\nu}^c$ and $\tilde{\ell}^c$ as the longitudinal components. Due to supersymmetry, one would expect that a corresponding large Dirac mass would develop between the $\nu^c - \tilde{Z}^0$ and $\ell^c - \tilde{W}_R^+$. Here we are interested in the chargino–lepton mixing, which is the new source of R-parity breaking effects. We explicitly write down the charged fermion mass matrix in the basis of $(\tilde{W}_R^+, \ell^{c+}) - (\tilde{W}_R^-, \ell^-)$,

$$M_C = \begin{bmatrix} M_{1/2} & 0 \\ M_{W_R} & m_\ell \end{bmatrix}, \quad (2.2)$$

where $M_{W_R} = g_R \langle \tilde{\nu}^c \rangle$ is the W_R gauge boson mass and $M_{1/2}$ is the soft SUSY breaking mass for the chargino. The (1-2) element is absent because neither the RH neutrino nor the Higgs VEV couples ℓ^- and \widetilde{W}_R^+ . The determinant of this mass matrix is proportional to the (light) charged lepton mass m_ℓ because the RH sneutrino VEV is an electroweak singlet and therefore does not break chirality. This means that there must be a physical state with the mass m_ℓ and identifiable as the charged lepton.

Diagonalization of this mass matrix leads to a mixing between ℓ^c and \widetilde{W}_R^+ . This mixing $\theta_{\ell W}$ is large if $M_{1/2} \simeq M_{W_R}$. The physical charged lepton state is then given by

$$\hat{\ell}^c = \theta_{\ell\ell} \ell^c + \theta_{\ell W} \widetilde{W}_R^+, \quad (2.3)$$

where $\theta_{\ell W} \sim \mathcal{O}(1)$. We note there is no such mixing induced for \widetilde{W}_R^- . Due to this mixing, one can derive two new classes of R-parity violating interactions from the right-handed gaugino matter coupling terms: First from the gaugino coupling $\sqrt{2}g\widetilde{W}_R^+ \nu_{\ell'}^c \tilde{\ell}'^{c\dagger} + \text{h.c.}$, we get

$$\mathcal{L}_{\text{new}}^{\ell'} = \sqrt{2}g\theta_{\ell W} \left[\hat{\ell}^c \nu_{\ell'}^c \tilde{\ell}'^{c\dagger} + \bar{\tilde{\ell}}^c \bar{\nu}_{\ell'}^c \tilde{\ell}'^c \right]. \quad (2.4)$$

Analogously, using the right-handed gaugino interaction with quarks and squarks, one can also write down the new RPV couplings for the squark-quark sector

$$\mathcal{L}_{\text{new}}^q = \sqrt{2}g\theta_{\ell W} \left[\hat{\ell}^c u^c \tilde{d}^{c\dagger} + \bar{\tilde{\ell}}^c \bar{u}^c \tilde{d}^c \right]. \quad (2.5)$$

Notice there is no supersymmetric counterpart of above terms generated, unlike those from the superpotential: $\lambda L L e^c$, $\lambda' Q L d^c$, etc.. The new couplings we obtain here break not only R-parity but also supersymmetry, since we started from a mass matrix Eq. (2.2) including the SUSY breaking gaugino mass.

As we will point out in Sec. 5, the most stringent constraints on the couplings in Eq. (2.5) are from neutrinoless double beta decay and HERA experiment [15], which tend to push the squark and gluino masses to TeV. On the other hand, the LEP2 Z-pole observables give a universal constraint [16] on the mixing parameter $\theta_{\ell W}$ in both Eqs. (2.4) and (2.5), but it turns out to be rather mild. Therefore, the sleptons masses are still allowed to be not far above 100 GeV.

From these new interactions derived from dynamical R-parity breaking, one would expect the following distinctive signatures at the LHC.

- Single production of slepton NLSP via Eq. (2.4) and subsequent decays (see Fig. 1), which is the main topic being studied in this paper.
- Top quark produced from down-type squark decay via Eq. (2.5), whose polarization is opposite to the components from the SM background, as well as the conventional λ' term.

We want to point out that these predictions are common to the models with R-parity broken together with extended gauge symmetries, as well as to those breaking $SU(2)_R$ symmetry without the Higgs triplets, as long as the RH neutrino mass lies in the proper range.

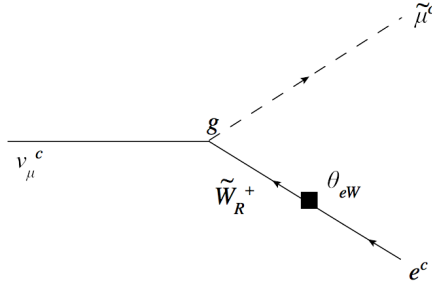


Figure 1. Single production of RH slepton from RH sneutrino decays. The black box represents RPV $e^c - \widetilde{W}_R^+$ mixing.

3 An Explicit Model of Dynamical R-parity Breaking

In this section, we present a model based on the group $SU(2)_L \times SU(2)_R \times U(1)_{B-L}$ where in the absence of R-parity breaking, the gauge symmetry does not break[2]. Thus the gauge dynamics dictates R-parity breaking. Hence it explicitly provides an example for dynamical R-parity breaking ¹.

The model considered in this section does not have the discrete parity symmetry. In the appendix, we will comment if such model can be built in a completely parity symmetric form. Here, we first review the salient features of the $SU(2)_L \times SU(2)_R \times U(1)_{B-L}$ model (without parity symmetry) for completeness and show how dynamical R-parity breaking occurs.

3.1 SUSYLR: No gauge symmetry breaking without R-parity breaking

The minimal SUSYLR model has the gauge group $G_{LR} = SU(3)_c \times SU(2)_L \times SU(2)_R \times U(1)_{B-L}$. The particle content and their representations under the gauge group for the completely parity symmetric case are listed in Table 1. The $SU(2)_R$ Higgs triplets Δ^c , $\bar{\Delta}^c$ have been introduced to give mass to the RH neutrinos and facilitate the seesaw mechanism. For the sake of simplicity, we assume that the left-handed triplets Δ , $\bar{\Delta}$ are decoupled at high scale and do not exist in the TeV theory. The superpotential of the model is

$$\begin{aligned}
 W = & Y_u Q^T \tau_2 \Phi_1 \tau_2 Q^c + Y_d Q^T \tau_2 \Phi_2 \tau_2 Q^c \\
 & + Y_\nu L^T \tau_2 \Phi_1 \tau_2 L^c + Y_l L^T \tau_2 \Phi_2 \tau_2 L^c + if (L^{cT} \tau_2 \Delta^c L^c) \\
 & + \mu_{\Phi ab} \text{Tr} (\Phi_a^T \tau_2 \Phi_b \tau_2) + \mu_\Delta \text{Tr} (\Delta^c \bar{\Delta}^c) , \tag{3.1}
 \end{aligned}$$

where Y 's are Yukawa couplings, f is the Majorana coupling of leptons and μ_Δ is the μ -term for triplets. Note that in the model there is no gauge singlets introduced.

¹For recent papers where hidden dynamics breaks R-parity, see [17] and also some experimental implications of such models see [18]. However, in these works, the R-parity is not broken together with extended gauge symmetries that couple to SM fermions, and therefore, does not predict the phenomenology of dynamical R-parity breaking being discussed in this paper.

	$SU(3)_c$	$SU(2)_L$	$SU(2)_R$	$U(1)_{B-L}$
Q	\square	\square	$\mathbf{1}$	$1/3$
Q^c	$\bar{\square}$	$\mathbf{1}$	\square	$-1/3$
L	$\mathbf{1}$	\square	$\mathbf{1}$	-1
L^c	$\mathbf{1}$	$\mathbf{1}$	\square	1
$\Phi_{1,2}$	$\mathbf{1}$	\square	\square	0
Δ^c	$\mathbf{1}$	$\mathbf{1}$	$\square\square$	-2
$\bar{\Delta}^c$	$\mathbf{1}$	$\mathbf{1}$	$\square\square$	2
Δ	$\mathbf{1}$	$\square\square$	$\mathbf{1}$	2
$\bar{\Delta}$	$\mathbf{1}$	$\square\square$	$\mathbf{1}$	-2

Table 1. Particle content in the minimal SUSYLR model. In this section, we first concentrate on the case with the left-handed Higgs triplets Δ , $\bar{\Delta}$ do not exist in the TeV theory for simplicity. We will comment on the fully parity symmetric theory in the appendix.

The corresponding soft terms are

$$\begin{aligned}
V_{\text{soft}} = & m_Q^2 \left(\tilde{Q}^\dagger \tilde{Q} + \tilde{Q}^{c\dagger} \tilde{Q}^c \right) + m_l^2 \left(\tilde{L}^\dagger \tilde{L} + \tilde{L}^{c\dagger} \tilde{L}^c \right) + m_\Delta^2 \text{Tr}(\Delta^{c\dagger} \Delta^c) + m_{\bar{\Delta}}^2 \text{Tr}(\bar{\Delta}^{c\dagger} \bar{\Delta}^c) \\
& + \frac{1}{2} (M_{2L} \lambda_L^a \lambda_L^a + M_{2R} \lambda_R^a \lambda_R^a + M_1 \lambda_{BL} \lambda_{BL} + M_3 \lambda_g \lambda_g) \\
& + \tilde{Q}^T \tau_2 A_i^q \phi_i \tau_2 \tilde{Q}^c + \tilde{L}^T \tau_2 A_i^\ell \phi_i \tau_2 \tilde{L}^c + i A_f \tilde{L}^{cT} \tau_2 \Delta^c \tilde{L}^c \\
& + B_{\Phi ab} \text{Tr}(\tau_2 \phi_a^T \tau_2 \phi_b) + B_\Delta \text{Tr}(\Delta^c \bar{\Delta}^c) + \text{h.c.} .
\end{aligned} \tag{3.2}$$

The D-term potential as well as the scalar potential can be found in Refs. [2, 9].

The desired symmetry breaking pattern is $SU(2)_R \times U(1)_{B-L} \rightarrow U(1)_Y$ at the first step, giving definite meaning to the hypercharge $Y = I_{3R} + (B - L)/2$, followed by the electroweak symmetry breaking. The key point to note is that the potential does not break any gauge symmetry in supersymmetric limit [19]. Even if the soft SUSY breaking terms are included, the gauge symmetry still remains unbroken as long as the RH sneutrino has zero VEV. Parity and $SU(2)_R \times U(1)_{B-L} \rightarrow U(1)_Y$ breaking become possible only if the RH sneutrino picks up a non-zero VEV. The RH sneutrino being superpartner field has odd R-parity and therefore its VEV breaks R-parity – hence the claim [2] that there is no parity breaking without R-parity breaking in the minimal SUSYLR model. Furthermore, it was shown in [6] that RH sneutrino VEV is tied to the soft mass scale M_{SUSY} . This implies an upper bound on the W_R gauge boson mass of order of the SUSY breaking scale.

To see this explicitly, we write down the potential including all VEV's given below;

$$\langle \tilde{L}_e^c \rangle = \begin{bmatrix} \langle \tilde{\nu}_e^c \rangle \\ 0 \end{bmatrix}, \quad \langle \Delta^c \rangle = \begin{bmatrix} 0 & 0 \\ v_R & 0 \end{bmatrix}, \quad \langle \bar{\Delta}^c \rangle = \begin{bmatrix} 0 & \bar{v}_R \\ 0 & 0 \end{bmatrix}, \tag{3.3}$$

where we choose to break the R-parity along the RH electron sneutrino $\tilde{\nu}_e^c$ direction, for phenomenological consideration to be explained in Section 3.2. The scalar potential involving

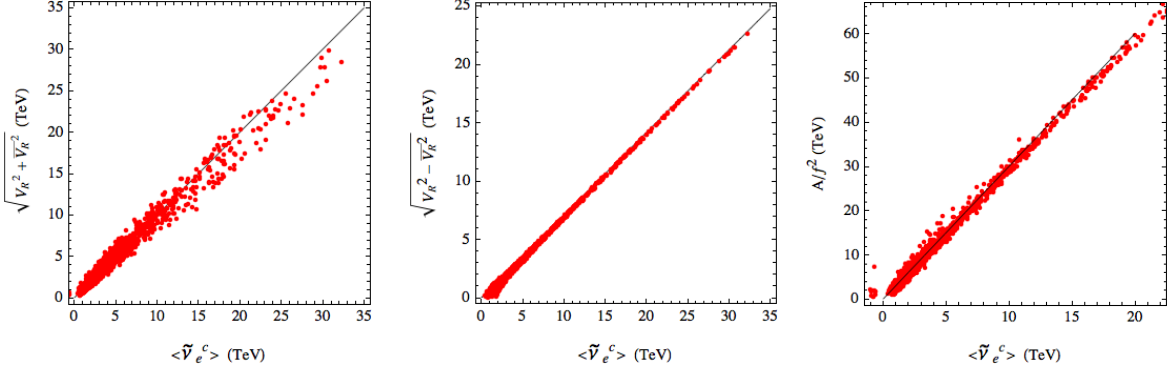


Figure 2. Correlations among the VEVs. The left-panel tells us that R-parity is broken as much as parity, $\langle \tilde{\nu}_e^c \rangle^2 \approx v_R^2 + \bar{v}_R^2$. The middle panel shows that the minimum always points towards the flat D-term potential direction, $\langle \tilde{\nu}_e^c \rangle^2 = 2(v_R^2 - \bar{v}_R^2)$. The right panel tells the value of the VEV is related to parameters in the potential as $\langle \tilde{\nu}_e^c \rangle \approx A/3f^2$. This agrees with the upper bound obtained in Ref. [9].

the Higgs triplets and RH sneutrinos is

$$\begin{aligned}
V = & M_1^2 v_R^2 + M_2^2 \bar{v}_R^2 - 2B v_R \bar{v}_R + |f|^2 \langle \tilde{\nu}_e^c \rangle^4 + \left[4|f|^2 v_R^2 + m_0^2 - 2|A|v_R - 2|f|\mu_\Delta \bar{v}_R \right] \langle \tilde{\nu}_e^c \rangle^2 \\
& + \frac{1}{8}(g^2 + g'^2)(\langle \tilde{\nu}_e^c \rangle^2 - 2v_R^2 + 2\bar{v}_R^2)^2, \tag{3.4}
\end{aligned}$$

where $M_1^2 = \mu_\Delta^2 + m_\Delta^2$, $M_2^2 = \mu_{\bar{\Delta}}^2 + m_{\bar{\Delta}}^2$ and $B = B_\Delta$. For simplicity, we have assumed the matrices f , A_f , m_ℓ^2 to be flavor diagonal and $f = f_{ee}$, $A = (A_f)_{ee}$ and $m_0^2 = (m_\ell^2)_{ee}$. The VEVs of the Higgs bidoublets have been neglected in the first stage of symmetry breaking. The potential should satisfy $B < M_1 M_2$ to be bounded from below. This can be seen by considering D-flat directions $\langle \tilde{\nu}_e^c \rangle = 0$, $\langle \Delta \rangle = \langle \Delta^c \rangle = v\tau_1$ and $\langle \bar{\Delta} \rangle = \langle \bar{\Delta}^c \rangle = \bar{v}\tau_1$, where τ_1 is the Pauli matrix. This scalar potential has the property that on $\langle \tilde{\nu}_e^c \rangle = 0$ surface, there is no symmetry breaking, i.e., $v_R = \bar{v}_R = 0$ at the minimum. The acceptable minimum that breaks parity and the gauge symmetries therefore necessarily breaks R-parity.

We have carried out numerical study of the minimization of the scalar potential, by scanning over the bulk of parameter space $(M_1, M_2, \sqrt{B}, A, \mu_\Delta, m_0) \in [100, 1000]$ GeV and $f \in [0.1, 0.5]$. The true vacuum must satisfy $V_{\min} < 0$ and $\langle \tilde{\nu}_e^c \rangle \neq 0$. It turns out that there are interesting correlations among the VEVs of RH neutrino and the Higgs fields. They are shown in Fig. 2. Typically, we find the D-term potential always vanishes, i.e., $\langle \tilde{\nu}_e^c \rangle^2 = 2(v_R^2 - \bar{v}_R^2)$. Therefore, the physics at the RH scale does not bring additional terms to the Higgs potential. The sneutrino VEV and the Higgs triplets VEV's are of the same order, $\langle \tilde{\nu}_e^c \rangle^2 \approx v_R^2 + \bar{v}_R^2$, as well as an approximate relation $\langle \tilde{\nu}_e^c \rangle \approx A/3f^2$. This agrees with the upper bound obtained in Ref. [9]. The key point is that, in SUSYLR model, the right-handed scale is dynamically generated through the SUSY breaking soft mass scale [2],

$$v_R \lesssim \frac{M_{\text{SUSY}}}{f^2}, \tag{3.5}$$

where $M_{\text{SUSY}} \sim \mathcal{O}(100)$ GeV corresponds to the generic soft SUSY breaking mass scale.

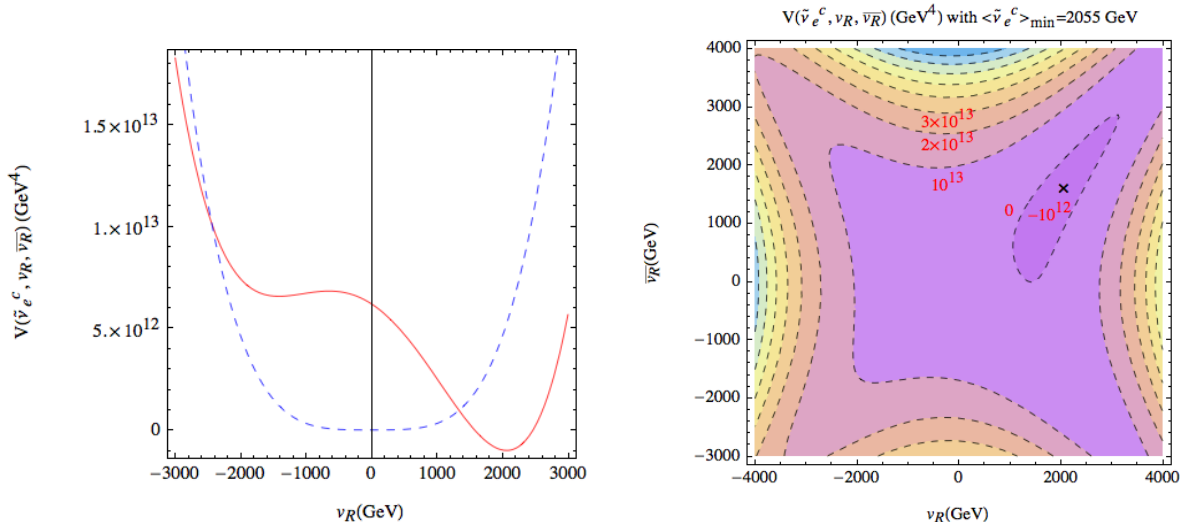


Figure 3. Left panel: The potential V as a function of ν_R for given $\langle \tilde{\nu}_e^c \rangle = 2055$ GeV, $\bar{\nu}_R = 1607$ GeV (solid curve) and $\langle \tilde{\nu}_e^c \rangle = \bar{\nu}_R = 0$ (dashed curve). Right panel: Contour plot of the potential V in the $\nu_R - \bar{\nu}_R$ plane for $\langle \tilde{\nu}_e^c \rangle = 2055$ GeV.

In order to illustrate the role of R-parity violation in symmetry breaking, we choose the following set of parameters

$$\begin{aligned}
 M_1 &= 213 \text{ GeV}, M_2 = 251 \text{ GeV}, \sqrt{B} = 150 \text{ GeV}, \\
 \mu_\Delta &= 517 \text{ GeV}, A = 240 \text{ GeV}, m_0 = 376 \text{ GeV}, f = 0.21 \quad .
 \end{aligned}
 \tag{3.6}$$

The resulting VEV's and the minimum potential value are

$$\langle \tilde{\nu}_e^c \rangle = 2055 \text{ GeV}, \quad \nu_R = 2063 \text{ GeV}, \quad \bar{\nu}_R = 1607 \text{ GeV}, \quad V_{\min} = -1.0 \times 10^{12} \text{ GeV}^4 \quad . \tag{3.7}$$

The configuration of the potential around the vacuum is shown in Fig. 3. Clearly, the global minimum of the potential breaks R-parity, i.e., $\langle \tilde{\nu}_e^c \rangle \neq 0$. Because the R-parity and the lepton number are broken simultaneously with the gauge symmetries, no massless Majoron is present. On the other hand, the dynamical R-parity breaking associated with gauge symmetry breaking at few TeV scale offers rich phenomenology.

3.2 Neutrino mass and flavor alignment of R-parity violation

Neutrino masses in this model have been discussed extensively in [9]. We review the salient points for completeness and, in particular, constraints on flavor of the R-parity violation. In SUSYLR model, the matter fields obtain their Dirac masses from the coupling to the Higgs bidoublets $\Phi_{1,2}$. Generally, there are four $SU(2)_L$ Higgs doublets at the electroweak scale. The additional neutral Higgs bosons will lead to flavor changing neutral currents at tree level.

This can be suppressed either by proper doublet-doublet splitting or by cancellations [20]. Another way to avoid the flavor changing Higgs effects is by replacing the second $B - L = 0$ bidoublet with a $B - L = 2$ bidoublet as has recently been suggested [21]. We do not discuss this here.

We assume that the bidoublet Higgs fields take the following form of VEV's,

$$\Phi_1 = \begin{bmatrix} 0 & 0 \\ 0 & \kappa_1 \end{bmatrix}, \quad \Phi_2 = \begin{bmatrix} \kappa_2 & 0 \\ 0 & 0 \end{bmatrix}, \quad (3.8)$$

where κ_1 gives Dirac masses to the up-type quarks and neutrinos, while κ_2 contributes to down-type quarks and charged leptons masses. With this VEV structure, the $W_L - W_R$ gauge bosons do not mix with each other. Here we mainly focus on the lepton sector. We will attribute the hierarchies among the charged lepton masses to the Yukawa couplings. In particular, we focus on the low $\tan\beta = \kappa_2/\kappa_1 \sim \mathcal{O}(1)$ regime. In this case, the Yukawa coupling constants are set as $y_\tau \approx 10^{-2}$, $y_\mu \approx 10^{-3}$, $y_e \approx 10^{-5.5}$ and $(Y_\nu)_{ij} \approx 10^{-6}$. Even though there are four SM Higgs doublets (or two MSSM Higgs pairs), since only two of them contribute to fermion masses and the other two play the role of spectators, our $\tan\beta$ is same as the MSSM one. The μ_Φ and B_Φ play a similar role as the μ and B_μ parameters in the MSSM for the electroweak symmetry breaking.

Because of R-parity violation, there are additional contributions to neutrino masses, on top of the Type-I seesaw mechanism. They arise from neutrino-neutralino mixing which has been calculated in Ref. [9] with R-parity breaking in the RH electron sneutrino direction,

$$(M_\nu)_{ij} \approx -\frac{g_L^2 g'^2 \kappa_2^2}{2M_{2L} M_{\tilde{B}} (\mu_{11} \mu_{22} - \mu_{12}^2)} \left(\frac{M_{2L}}{g_L^2} + \frac{M_{2R}}{g_R^2} + \frac{M_1}{g_{BL}^2} \right) \times \left[\left(\frac{\mu_{12}}{\mu_{11}} \right) (Y_\nu)_{i1} (Y_\nu)_{1j} + (Y_\nu)_{i1} y_e \delta_{j1} + (Y_\nu)_{1j} y_e \delta_{i1} - \left(\frac{\mu_{11}}{\mu_{12}} \right) y_e^2 \delta_{i1} \delta_{j1} \right] \langle \tilde{\nu}_e^c \rangle^2, \quad (3.9)$$

assuming the LH sneutrino VEV's are negligible. $M_{L,R}$ and M_{BL} are soft supersymmetry breaking gaugino masses. The corresponding Feynman diagram is shown in the left panel of Fig. 4. Choosing the R-parity violation along the $\tilde{\nu}_e^c$ direction helps to avoid too large contributions through the y_τ , y_μ couplings, while the electron and neutrino Yukawa couplings are sufficiently small to keep the neutrino mass scale $\mathcal{O}(0.1)$ eV in tact.

We also notice that there are radiative corrections to the neutrino mass [22, 23], which are also proportional to the corresponding Yukawa coupling and are loop suppressed (see the right panel of Fig. 4, as well as Fig. 2 in [24]). So they are safely small as long as $\langle \tilde{\nu}_\mu^c \rangle$ and $\langle \tilde{\nu}_\tau^c \rangle$ are vanishing and $\tan\beta$ is low.

The above discussions justify our choices of VEV configuration in Eq. (3.3).

Before closing this section, we comment on the flavor violations. The next section will mainly concentrate on the scenario with slepton NLSP singly produced from the W_R^\pm gauge boson resonance, hence we need to understand the existing experimental constraints on the

relevant mass scales. In the minimal non-SUSY left-right model, the famous neutral K -meson mixing tends to push to W_R mass to be above 2.4 TeV [25]. In the supersymmetric version, loop diagrams mediated by superpartners also make additional contribution to both quark and lepton flavor violation processes. They are safely small if the relevant mass scales are high enough. Otherwise, in order to optimize the discovery prospects at the LHC, the superpartners and W_R -boson masses have to lie in the (sub-)TeV regime, which requires fine-tuning the flavor structures of the model in a similar way to the MSSM. This is nothing but the SUSY flavor problem, and the constraints on scales are quite model dependent. In principle, there could also be contribution to flavor violations from higher dimensional operators controlled by unknown physics in the UV.

Therefore, in the following we shall only adopt the bounds $M_{W_R} > 1$ TeV and $m_{\tilde{\ell}} > 100$ GeV from Tevatron and LEP2 direct searches, respectively.

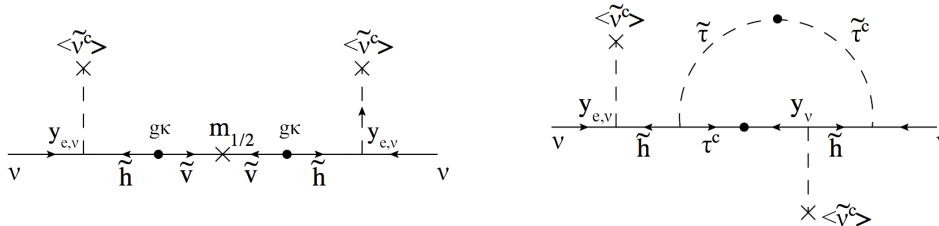


Figure 4. Contributions to neutrino masses from R-parity violation. Left panel: tree-level contribution due to neutrino-neutralino mixing. Right panel: loop-suppressed radiative correction to the neutrino masses. The $\tilde{\nu}$ represents neutral gaugino fields. The black dots are the usual Higgs VEV insertions.

4 Single Production of Slepton NLSP and its Decay at the LHC

In this section, we start exploring the LHC implications of this model. First we need to know the R-parity violating (RPV) interactions that induce the decays of the particles produced.

4.1 Relevant RPV couplings

In general, spontaneous R-parity breaking through the RH sneutrino VEV generates the bilinear terms in the superpotential and the soft potential

$$W_{\mathcal{R}} = \mu_i L_i H_u, \quad V_{\mathcal{R}\text{-soft}} = B_i \tilde{L}_i H_u + \text{h.c.} . \quad (4.1)$$

The bilinear term facilitates the R-parity breaking decay of the lightest neutralino, $\tilde{\chi}_1^0$ as follows: $\tilde{\chi}_1^0 \rightarrow Z^0 \nu$, $\tilde{\chi}_1^0 \rightarrow W^\pm \ell_\mp$ or $\tilde{\chi}_1^0 \rightarrow \ell_1^+ \ell_2^- \nu$ [5]. In the literature, more complete collider phenomenologies of R-parity violation from the superpotential has been studied in detail and reviewed in Refs. [22, 26–28].

In the SUSYLR model, the bilinears arise from the electron and neutrino Yukawa couplings and the corresponding A -term once the RH sneutrino VEV is inserted [9]. Therefore

$$\frac{\mu_i}{\mu_\Phi} \simeq \frac{B_i}{B_\Phi} \simeq y_e, y_\nu \simeq 10^{-6} . \quad (4.2)$$

These bilinear terms will induce trilinear R-parity breaking terms $\lambda LLe^c, \lambda' QLd^c$. The most important terms for the following study are those associated with third generation fermions,

$$\lambda'_i t \ell_i b^c + \lambda_i \nu \ell_i \tau^c , \quad (4.3)$$

where $\lambda'_i = y_i \mu_i / \mu_\Phi$, $\lambda_i = y_\tau \mu_i / \mu_\Phi$ and $i = 1, 2, 3$. On the other hand, the λ'' term will not be generated, since baryon number symmetry is respected by the sneutrino VEV, thereby guarantee the proton stability.

As already stated in previous sections, a distinct feature that arises when R-parity is dynamically broken together with an $SU(2)_R$ gauge symmetry is the large mixing between the RH electron e^c and the $SU(2)_R$ gaugino, i.e., \widetilde{W}_R^+ . This is not present in the MSSM with general R-parity violation. The form of charged fermion mass matrix and the obtained mixing in SUSYLR model is given explicitly in the Appendix. From the usual gaugino Yukawa-like coupling term for μ and τ flavors, one obtains the new couplings (similar to Eq. (2.4))

$$\mathcal{L}_{\text{new}}^\ell = \sqrt{2} g \theta_{eW} \left[e^c \nu_\mu^c \widetilde{\mu}^{c\dagger} + \bar{e}^c \bar{\nu}_\mu^c \widetilde{\mu}^c \right] + \sqrt{2} g \theta_{eW} \left[e^c \nu_\tau^c \widetilde{\tau}^{c\dagger} + \bar{e}^c \bar{\nu}_\tau^c \widetilde{\tau}^c \right] . \quad (4.4)$$

As we will see, these interactions open new channel for the single production of a slepton at hadron colliders (Fig. 1). Similarly, from the neutralino mass matrix, one can also obtain large mixing between the \widetilde{Z}' and ν_e^c , and in turn the couplings

$$\mathcal{L}_{\text{new}}^{\nu_e^c} = \sqrt{2} g_{Z'} \theta_{NZ'} \left(\nu_e^c \mu^c \widetilde{\mu}^{c\dagger} + \nu_e^c \tau^c \widetilde{\tau}^{c\dagger} + \nu_e^c \nu_\mu^c \widetilde{\nu}_\mu^{c\dagger} + \nu_e^c \nu_\tau^c \widetilde{\nu}_\tau^{c\dagger} \right) + \text{h.c.} . \quad (4.5)$$

In principle, sparticle single production could also happen through the mixing between ν_e^c and \widetilde{Z}' [24] which, however, calls for some tuning between $M_{Z'}$ and $M_{1/2}$.

Contrary to the usual R-parity breaking term from superpotential, these new R-parity breaking sources come from the gaugino Yukawa-like couplings (in the Kähler potential). As we illustrate in the below, such theories could be tested at the LHC where the new gauge interactions are accessible.

4.2 Branching ratios of slepton NLSP decay

From the previous sections one learns that, in the SUSYLR model under discussion, a new class of RPV couplings Eq. (4.4) emerge due to the mixing between e^c and \widetilde{W}_R^+ . To study its implications for hadron colliders, we need to know the sparticle spectrum. If one takes the assumption of universal scalar masses at high scale, the RH sleptons are likely to be the lightest among matter superpartners in the MSSM due to the smaller Yukawa couplings as well as the smaller weak gauge couplings [29]. The situation would be similar in SUSYLR models.

The lightest slepton could be a stau or the smuon depending on detailed parameter range. In our study, we will assume that smuon is the lightest superpartner above the gravitino, the latter in our model could be the very weakly unstable dark matter.

As promised, we study the implications of scenario at the LHC for the case where smuon or stau is the NLSP among the superpartners. Due to the relatively low tagging efficiency of the tau lepton, we would focus on the smuon.

The new LHC signals originate from the production of W_R in pp collision and its subsequent decay to muon and RH muon neutrino which subsequently decays. In the non-SUSY LR models with type I seesaw the RH neutrino decays mostly to the three body final state $\ell^\pm \ell^\pm jj$ via W_R exchange [30, 31]. However in the SUSY version, if the smuon, $\tilde{\mu}$ is lighter than ν^c , an interesting new two body final state channel emerges: RH neutrino decays to a $\tilde{\mu}$ and an electron. Since this is two-body decay, for the smuon sufficiently light, it will certainly dominate over the three body non-SUSY mode,² as shown in Fig. 5. Therefore, the smuon single production could take this advantage and be large enough to be probed at the LHC.

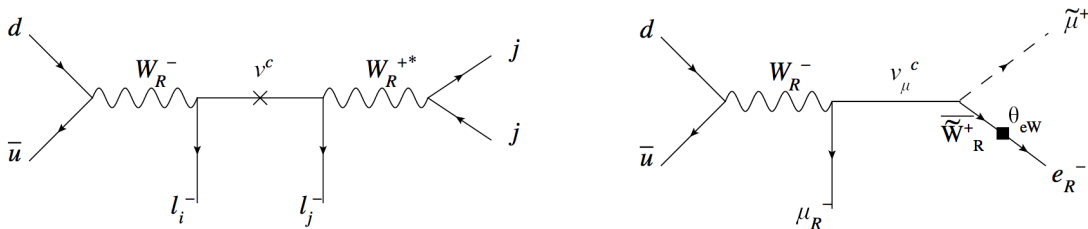


Figure 5. Production of the RH neutrino and its decays. Left-panel: the usual same-sign lepton diagram for W_R discovery. Right-panel: Single production of the smuon through RH neutrino RPV decay. In this case, there is equal possibility to break the muon lepton number twice through the Majorana mass of ν_μ^c or not, so one can get either $\tilde{\mu}^+ e_R^-$ or $\tilde{\mu}^- e_R^+$ from its decay. The black box represents sneutrino VEV insertion as indicated in Fig. 1.

As the NLSP, the smuon $\tilde{\mu}_{\text{NLSP}} = \cos \alpha \tilde{\mu}_R + \sin \alpha e^{i\beta} \tilde{\mu}_L$ will decay dominantly through R-parity breaking interactions rather than the Planck scale suppressed decay to the gravitino. In the case where there is a large mixing between LH and RH smuons, i.e., $\sin \alpha \sim \mathcal{O}(1)$, $\tilde{\mu}^+$ can decay to $t\bar{b}$ or $\tau\bar{\nu}$ through the induced trilinear RPV terms as shown in Eq. (4.3), although suppressed by the small y_e or y_ν Yukawa couplings. Note that electroweak symmetry forbids the direct coupling of RH smuon to $\bar{f}f$, and the RH sneutrino VEV does not help because it is also a singlet. Only the LH and RH smuon mixing term $(m_\mu^2)_{LR}$ which is proportional to the Higgs doublet VEV, can facilitate this decay.

On the other hand, if the mixing term $(m_\mu^2)_{LR}$ is severely suppressed, i.e., $\sin \alpha \ll 1$, the smuon is almost purely RH. Therefore, it decays through a four-body channel, as shown in the right panel of Fig. 6. Such decay rate is proportional to the gauge coupling instead of the

²Since the RH neutrino mass matrix is proportional to the matrix f , which we have taken to be diagonal in the basis of physical charged leptons, there is no further flavor changing in ν^c mass matrix (propagator).

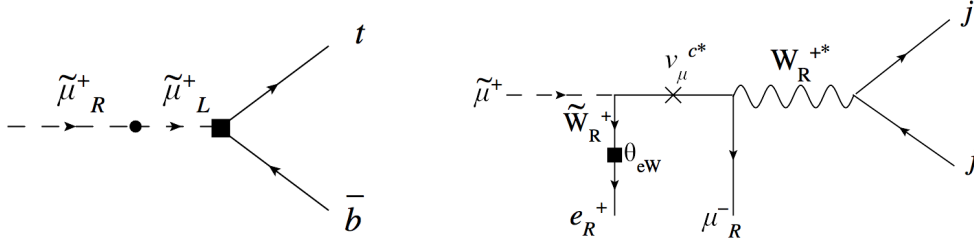


Figure 6. Two- and four-body decay modes of the smuon NLSP. The black box represents sneutrino VEV insertion as indicated in Fig. 1. The black dot stands for the usual Higgs VEV insertions. Hereafter, we denote the RH smuon as $\tilde{\mu}^c \equiv \tilde{\mu}_R^+$.

small y_e or y_ν couplings. It could be comparable or even dominate over the above two-body decays when the latter is further suppressed by the LR smuon mixing. In principle, $\tilde{\mu}^c$ can decay to both $e^+\mu^\pm jj$ final states. However, since the intermediate RH neutrino is off-shell, the probability to break the muon lepton number is larger than that conserving the lepton number. This point can be seen from the blue and brown curves in the left panel of Fig. 7.

The branching ratios to different final states of the smuon decay has been plotted in Fig. 7 with the following parameters chosen, $M_{W_R} = 2 \text{ TeV}$, $M_{\nu_\mu^c} = 500 \text{ GeV}$ and $g\theta_{eW} = 0.2$. In the suppressed LR slepton mixing case (left panel, here and below, we will take $\sin \alpha \approx 10^{-3}$ as a benchmark point), the four-body decay of smuon NLSP always dominates over all the two-body channels. In the large mixing case (right panel), the $t\bar{b}$ channel will dominate if it is kinematically allowed, while $\tau\bar{\nu}$ and the four-body channels $e^+\mu^- jj$ could respectively dominate in certain low smuon mass windows. In both cases, since the Majorana RH neutrinos are involved in the production and/or decay processes, lepton number can be broken, which leads to the most promising discovery channels at the LHC. The expected signatures are listed in Table 2.

	large $\tilde{\mu} - \tilde{\mu}^c$ mixing	suppressed mixing
$M_{\tilde{\mu}^c} > m_t + m_b$	$pp \rightarrow \mu^- e^- t\bar{b}, \mu^+ e^+ t\bar{b}$	$pp \rightarrow \mu^\pm \mu^\pm e^+ e^- jj$
$M_{\tilde{\mu}^c} < m_t + m_b$	$pp \rightarrow \mu^\pm \mu^\pm e^+ e^- jj$ $pp \rightarrow \mu^- e^+ \tau^+ + \cancel{E}_T$	

Table 2. Expected final states in the single production of the NLSP $\tilde{\mu}^c$ with $M_{\tilde{\mu}^c} < M_{\nu^c}$ assumed. Large and suppressed $\tilde{\mu} - \tilde{\mu}^c$ mixing cases are both listed.

In the following two subsections we will discuss the signature of the single production and decay of smuon NLSP via a heavier right-handed neutrino. We also discuss possible standard model backgrounds and elaborate on the selection criteria necessary for such signals to be significantly observed over the standard model background. The large number of diagrams involved in the standard model background processes are calculated using the helicity am-

plitude package MadGraph [32] and CalcHEP 2.5.4 [33]. To estimate the number of signal and background events as well as their phase space distribution(s), we use a parton-level Monte-Carlo event generator. In our numerical analysis, we use the CTEQ6L parton distribution function [34] and fix the factorization scale $Q^2 = \hat{s}/4$. In our parton-level simulation of both signal and background events, we smear the leptons and jet energies with a Gaussian distribution according to

$$\frac{\delta E}{E} = \frac{a}{\sqrt{E/\text{GeV}}} \oplus b \quad (4.6)$$

with the CMS parameterization, $a_\ell = 5\%$, $b_\ell = 0.55\%$ and $a_j = 100\%$, $b_j = 5\%$, \oplus denotes a sum in quadrature.

4.3 $pp \rightarrow e^+e^-\mu^\pm\mu^\pm jj$

This particular final state dominates when the mixing between LH and RH smuon is suppressed (or in the low mass ($\lesssim M_{\text{top}}$) region for a large mixing). In this section, we will denote smuon NLSP as $\tilde{\mu}^c$ since it is mainly the RH component. The most striking feature of this final state is the *three same sign leptons* and one opposite sign lepton associated with two jets without missing energy. Assuming the narrow width approximation for ν^c and $\tilde{\mu}^c$, we can simply write down the signal cross-section $\sigma_s(pp \rightarrow e^+e^-\mu^+\mu^+jj)$ as

$$\begin{aligned} \sigma(pp \rightarrow e^+e^-\mu^+\mu^+jj) &\approx \sigma(pp \rightarrow W_R^+ \rightarrow \mu^+\nu_\mu^c) \\ &\times \left[\text{Br}(\nu_\mu^c \rightarrow \tilde{\mu}^c e^-) \times \text{Br}(\tilde{\mu}^c \rightarrow e^+\mu^c jj) + \text{Br}(\nu_\mu^c \rightarrow \tilde{\mu}^{c\dagger} e^+) \times \text{Br}(\tilde{\mu}^{c\dagger} \rightarrow e^-\mu^+ jj) \right], \end{aligned} \quad (4.7)$$

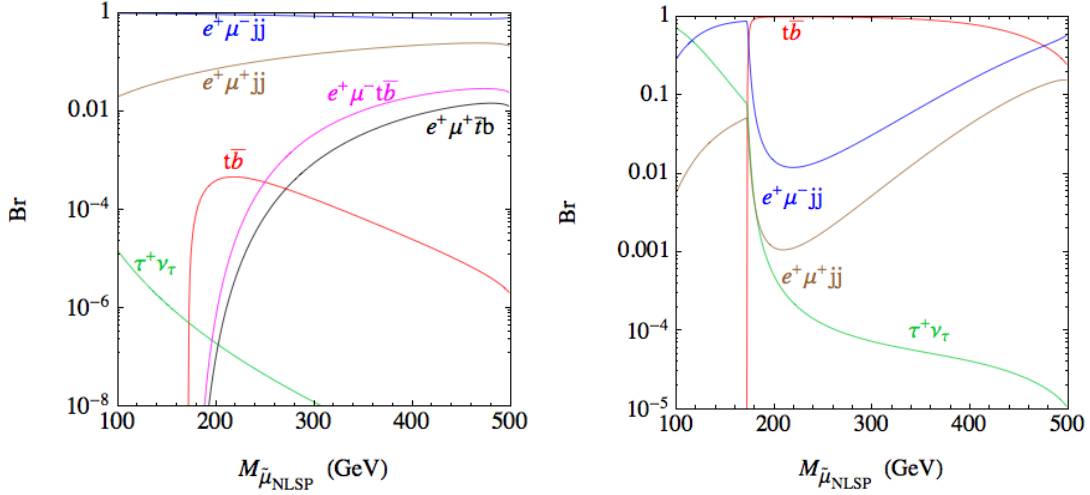


Figure 7. Branching ratios for the smuon NLSP decay. The left panel represents the suppressed LH and RH slepton mixings ($\sim 10^{-3}$) case, while in the right panel, we take an unsuppressed $\mathcal{O}(1)$ such mixing. Charge conjugated final states are not listed but also possible.

where the red (dotted) arrow indicates lepton number violation by two units on the involved RH neutrino propagator. The charge conjugated final state $\sigma(pp \rightarrow e^+ e^- \mu^- \mu^- jj)$ which is mediated by the intermediate W_R^- boson can be similarly approximated. In our analysis, we combine both these two final states. We define the signal identification with four charged leptons and two jets. The events are further selected by the following set of cuts

1. We require that both jets and leptons should appear within the detector's rapidity coverage, namely

$$|\eta(\ell)| < 2.5, \quad |\eta(j)| < 3. \quad (4.8)$$

2. The leptons are ordered according to their transverse momentum (p_T) hardness and the p_T of the leading lepton must satisfy

$$p_T(\ell_1) > 100 \text{ GeV} , \quad (4.9)$$

and for rest of the leptons

$$p_T(\ell) > 15 \text{ GeV} . \quad (4.10)$$

For two associated jets we demand that

$$p_T^{\text{jets}} > 25 \text{ GeV} . \quad (4.11)$$

3. We must also ensure that the jets and leptons are well separated so that they can be identified as individual entities. To this end, we use the well-known cone algorithm defined in terms of a cone angle $\Delta R_{\alpha\beta} \equiv \sqrt{(\Delta\phi_{\alpha\beta})^2 + (\Delta\eta_{\alpha\beta})^2}$ with $\Delta\phi$ and $\Delta\eta$ being the azimuthal angular separation and rapidity difference between two particles. We demand that

$$\Delta R_{jj} > 0.4 , \quad \Delta R_{\ell j} > 0.4 , \quad \Delta R_{\ell\ell} > 0.4 . \quad (4.12)$$

4. In our analysis, We use simplified definition for the missing transverse energy: $\cancel{E}_T = \sqrt{(\sum p_x)^2 + (\sum p_y)^2}$, where the sum goes over all observed charged leptons and jets. We demand that there is no significant missing energy in our signal

$$\cancel{E}_T < 30 \text{ GeV} . \quad (4.13)$$

Our choice of p_T cut on the leading lepton (Eq. (4.9)) can be well justified from the p_T distribution of all four leptons as displayed in Fig. 8 assuming $M_{W_R} = 1 \text{ TeV}$, $M_{\nu_{\tilde{e}}^c} = 500 \text{ GeV}$ and $M_{\tilde{\mu}^c} = 300 \text{ GeV}$ and at $\sqrt{s} = 14 \text{ TeV}$. Here, one should note that while generating p_T distributions (Fig. 8), we impose an uniform loose cut ($p_T > 15 \text{ GeV}$) on all four leptons, however, rest of the cuts remain unchanged. From the choice of mass parameters and simple kinematics of the production and decay chain, it is very obvious that the leading lepton (ℓ_1) comes from the two body decay of heavy $W_R^+ \rightarrow \mu^+ + \nu_{\mu}^c$, while rest of the leptons originating from the cascade decay chain of ν^c and $\tilde{\mu}^c$ have relatively softer transverse momentum

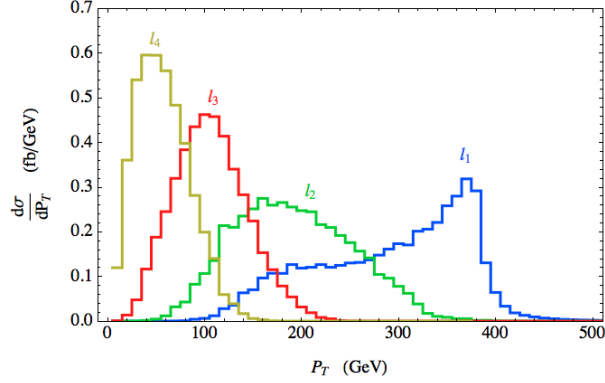


Figure 8. p_T distributions of all four leptons in the process $pp \rightarrow e^+e^-\mu^\pm\mu^\pm jj$ at $\sqrt{s} = 14$ TeV. The leptons are ordered according to their p_T hardness ($p_T(\ell_1) > p_T(\ell_2) > p_T(\ell_3) > p_T(\ell_4)$). We have fixed $M_{W_R} = 1$ TeV, $M_{\nu_\mu^c} = 500$ GeV, and $M_{\tilde{\mu}^c} = 300$ GeV.

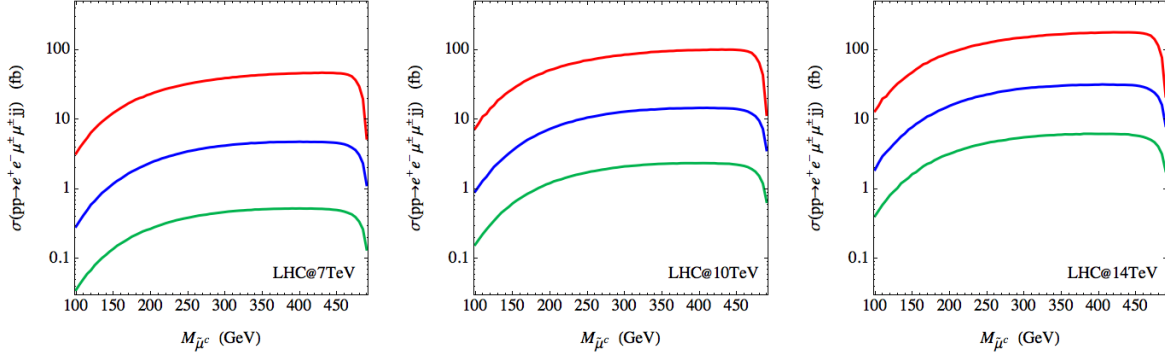


Figure 9. Signal cross sections $\sigma(pp \rightarrow e^+e^-\mu^\pm\mu^\pm jj)$ (after all cuts as mentioned in the text) as a function of smuon mass at the LHC with $\sqrt{s} = 7$ TeV, 10 TeV and 14 TeV. Three curves from top to bottom in each panel correspond to $M_{W_R} = 1$ TeV, 1.5 TeV and 2 TeV respectively. $M_{\nu_\mu^c}$ is kept fixed at 500 GeV.

compared to the p_T of the leading lepton. On the other hand, as the RH neutrino mass is increased to a value closer to the W_R mass, the first lepton becomes softer. However, in this case, the lepton from the decay $\nu_\mu^c \rightarrow e^-\tilde{\mu}^c$ merits the highest p_T and will serve as the hardest lepton (ℓ_1).

In Fig. 9 we show the total signal cross-section σ_s (after imposing all the cuts mentioned above) for the process shown in Eq. (4.8), as a function of the smuon $\tilde{\mu}^c$ mass at the LHC for 7 TeV, 10 TeV and 14 TeV energies. In each panel, three curves from top to bottom correspond to $M_{W_R} = 1$ TeV, 1.5 TeV and 2 TeV respectively. We fix the RH neutrino mass $M_{\nu_\mu^c} = 500$ GeV and the mixing parameter $g\theta_{eW} = 0.2$ for the present analysis. Before estimating the possible Standard Model backgrounds to this particular channel, we would like to discuss the

general behaviour of the signal cross sections.

- In all three panels, irrespective of M_{W_R} , the σ_s first rises with the increases of smuon mass and then becomes almost flat and finally drops sharply as $M_{\tilde{\mu}^c}$ becomes degenerate with right-handed neutrino mass $M_{\nu_\mu^c}$.
- The initial rise of the cross-section with the smuon mass can be understood from the fact that for lighter smuon mass ($M_{\tilde{\mu}^c} \sim 100 - 200$ GeV), the decay products of smuons $\tilde{\mu}^c \rightarrow e^+ \mu^+ jj$ are more collimated and fail to satisfy our isolation criteria for leptons and jets as shown in Eq. (4.12). As the smuon mass increases, leptons and jets which originate from the cascade decay of smuon tend to appear with larger ΔR , thus satisfying the isolation criteria as displayed in Eq. (4.12). As a consequence, the σ_s for heavier smuon mass ($M_{\tilde{\mu}^c} \lesssim M_{\nu_\mu^c}$) is significantly larger than for lower smuon mass region.
- The signal cross section σ_s strongly depends on \sqrt{s} , mass M_{W_R} and off course on $M_{\tilde{\mu}^c}$. There is a possibility that the LHC may also run at $\sqrt{s} = 10$ TeV, before attaining to its designed $\sqrt{s} = 14$ TeV. Keeping this in mind, we decided to provide our observation for $\sqrt{s} = 10$ TeV also. It is very interesting to note that for all the choices of M_{W_R} and \sqrt{s} the smallest cross-section always correspond to $M_{\tilde{\mu}^c} = 100$ GeV, while the largest one correspond to $M_{\tilde{\mu}^c}$ which lies between 400 – 430 GeV as shown in Table 3.

M_{W_R}	7 TeV	10 TeV	14 TeV
1 TeV	3.2–46.8	7.0–100	13–178
1.5 TeV	0.3–4.7	0.9–14.6	1.0–31.7
2 TeV	0.035–0.5	0.1–2.3	0.4–6.2

Table 3. The range of minimum and maximum $\sigma(pp \rightarrow e^+ e^- \mu^\pm \mu^\pm jj)$ (fb) at the LHC for $\sqrt{s} = 7, 10, 14$ TeV and $M_{W_R} = 1, 1.5, 2$ TeV, respectively. The corresponding smuon masses are mentioned in the text. The other parameters are taken as $M_{\nu_\mu^c} = 500$ GeV and $g\theta_{eW} = 0.2$.

Mass reconstruction: The most important feature of our signal events is the effective reconstruction of all three heavy particle masses from the final state charged leptons and jets. We first select two softest leptons (satisfying our selection criteria) from the four lepton set and then recombine these two leptons with the two jets to reconstruct the smuon mass, $M_{jj\ell_3\ell_4} \approx M_{\tilde{\mu}^c}$. After the obtaining the smuon resonance, we attempt to reconstruct the RH neutrino mass by combining two jets, two softest leptons with one of the two hardest leptons ℓ_1 or ℓ_2 . In this case, we face the complication due to combinatorics with two choices of pairing for $\ell_{1,2}$ with $M_{jj\ell_3\ell_4}$. Finally, W_R can be reconstructed by combining all four charged leptons and two jets. In Fig. 10, we display the invariant mass distribution for $\tilde{\mu}^c, \nu_\mu^c$ and W_R at 7 TeV LHC. Fitting the mass distribution with a Gaussian, we get the following values

$$M_{\tilde{\mu}^c}^{\text{fit}} = 301.36 \pm 1.74 \text{ GeV}, \quad M_{\nu_\mu^c}^{\text{fit}} = 500.43 \pm 0.75 \text{ GeV}, \quad M_{W_R}^{\text{fit}} = 999.45 \pm 2.10 \text{ GeV}, \quad (4.14)$$

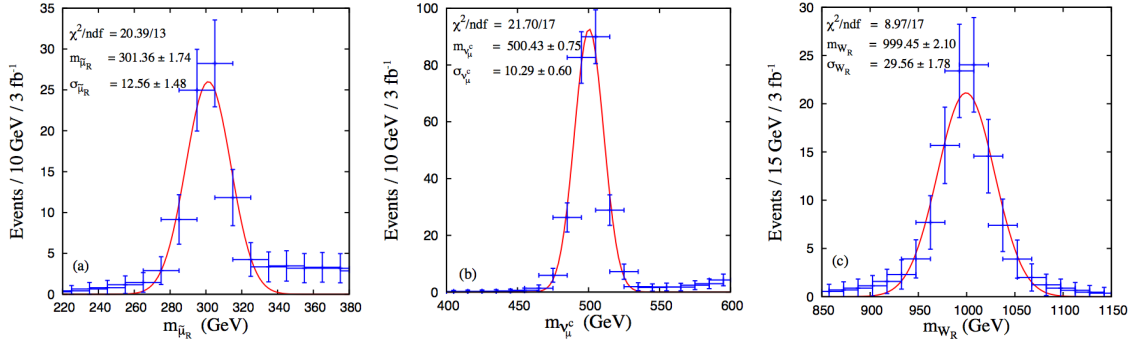


Figure 10. Invariant mass distributions for $M_{\tilde{\mu}^c}$, $M_{\nu_\mu^c}$ and M_{W_R} in the $pp \rightarrow e^+ e^- \mu^\pm \mu^\pm jj$ process at $\sqrt{s} = 7$ TeV with 3 fb^{-1} data for $M_{\tilde{\mu}^c} = 300$ GeV, $M_{\nu_\mu^c} = 500$ GeV and $M_{W_R} = 1$ TeV respectively. The error-bars shown are statistical only for the indicated luminosity. Results of Gaussian fitting are also shown.

where the input masses considered for this mass reconstruction procedure are the following

$$M_{\tilde{\mu}^c}^{\text{true}} = 300 \text{ GeV}, \quad M_{\nu_\mu^c}^{\text{true}} = 500 \text{ GeV}, \quad M_{W_R}^{\text{true}} = 1000 \text{ GeV}. \quad (4.15)$$

SM background	σ_0 (pb)	$\sigma_{\ell^\pm \ell^\pm}$ (fb)
$pp \rightarrow b\bar{b}b\bar{b}$	387.5	0.16
$pp \rightarrow t\bar{t}$	448	0.09
$pp \rightarrow Z^0 b\bar{b}$	0.051	3×10^{-5}
$pp \rightarrow W^\pm W^\pm W^\mp Z^0$	6.7×10^{-4}	2×10^{-5}
$\sigma_{\text{B}}^{\text{total}}$		0.25

Table 4. The list of leading-order SM backgrounds that could mimic our signal. σ_0 and $\sigma_{\ell^\pm \ell^\pm}$ are defined in the text. These numbers correspond to $\sqrt{s} = 14$ TeV.

SM backgrounds: In principle, there is no intrinsic standard model background to the $\Delta L = 2$ processes. However, there some standard model processes which could mimic our signal if the missing transverse momentum of neutrinos are balanced. One of the dominant background is $pp \rightarrow b\bar{b}b\bar{b}$, followed by semileptonic decay of all the b-quarks. We generate this background using with the following basic cuts $p_T(b) > 25$ GeV, $|\eta(b)| < 2.5$ and $\Delta R_{bb} > 0.4$. The leading order cross-section is 388 pb at $\sqrt{s} = 14$ TeV. After hadronization, one of the B^0 or \bar{B}^0 has to oscillate before decay, in order to get a pair of same-sign dileptons. The probability of having $b\bar{b} \rightarrow e^\pm \mu^\pm, \mu^\pm \mu^\pm$ is about $P_{\ell^\pm \ell^\pm}^{b\bar{b}} \approx 2 \times 10^{-5}$, as estimated in [35]. After taking into account the semileptonic branching ratio $\sim 10\%$ for the other two b-quarks we find this background cross-section $\sim 10^{-1}$ (fb). The other apparently looking very severe standard model background is $pp \rightarrow t\bar{t}$. At leading order, the top pair production cross-section ($\sigma_{t\bar{t}}$) is 448 pb at the LHC with $\sqrt{s} = 14$ TeV. After taking into account the leptonic branching

fraction of two W bosons (from $t \rightarrow bW^+$) and $P_{\ell^\pm\ell^\pm}^{b\bar{b}}$, the rate goes down to $\sim 10^{-1}$ (fb). Here, we would like to mention that if we take into account the higher order QCD effects, $\sigma_{t\bar{t}}$ becomes ≈ 900 (pb), which means our final background cross-section from $t\bar{t}$ process may increase atmost by a factor of two. The other sub-leading standard model processes which may fake our signal processes are $pp \rightarrow Zb\bar{b}$, $pp \rightarrow W^\pm W^\pm W^\mp Z^0$ and $pp \rightarrow W^\pm W^\pm W^\mp h$. In the case of $pp \rightarrow Zb\bar{b}$, process, $Z \rightarrow \ell^+\ell^-$, $\ell = e, \mu$ and same sign leptons will come from $b\bar{b}$ pair by oscillation of one of the B^0 meson before decay. As a result of this, the $\sigma(pp \rightarrow Zb\bar{b})$ will be suppressed by $\text{Br}(Z \rightarrow \ell^+\ell^-)$, $\ell = e, \mu$ and $P_{\ell^\pm\ell^\pm}^{b\bar{b}}$. The rate for same sign leptons from remaining two processes are negligibly small. In Table 4, we summarize the standard model background cross-sections, where, σ_0 and $\sigma_{\ell^\pm\ell^\pm}$ correspond to the leading order cross-sections before and after folding with different suppression factors arising from leptonic branching ratios of W^\pm, Z bosons, semi-leptonic branching ratio of $b(\bar{b})$ quark and finally $P_{\ell^\pm\ell^\pm}^{b\bar{b}}$ respectively. From this very simple minded exercise, we conclude that our signal is almost SM background free.

4.4 $pp \rightarrow \mu^\pm e^\pm b\bar{b}jj$

The smuon heavier than top quark and with large mixing L-R mixing $\mathcal{O}(1)$ can lead to this final state. Here we call the smuon NLSP as $\tilde{\mu}$, without definite chirality. As shown in Table 2, the smuon will dominantly decay to $t\bar{b}$ via the λ' coupling in this case. For this signal topology, we select events with *two same sign different flavoured* (SSDF) charged leptons and four jets. The cross section for this channel in the narrow width approximation can be expressed as

$$\sigma(pp \rightarrow \mu^+ e^+ b\bar{b}jj) \approx \sigma(pp \rightarrow W_R^+ \rightarrow \mu^+ \nu_\mu^c) \cdot \text{Br}(\nu_\mu^c \rightarrow \tilde{\mu}^- e^+) \cdot \text{Br}(\tilde{\mu}^- \rightarrow t\bar{b}) \cdot \text{Br}(\bar{t} \rightarrow \bar{b}jj). \quad (4.16)$$

The signal also includes the charge conjugated final state $\sigma(pp \rightarrow \mu^- e^- b\bar{b}jj)$ via intermediate W_R^- boson.

Our selection cuts are same as shown in Eqs. (4.8)–(4.13), except for the transverse momentum cut on the jets. After ordering all four jets according to their p_T , we impose following cut on the hardest jet (j_1):

$$p_T(j_1) > 60 \text{ GeV} \quad (4.17)$$

and for rest of the jets

$$p_T(j_2, j_3, j_4) > 25 \text{ GeV} . \quad (4.18)$$

In Fig. 11 we display the p_T distribution of two leptons and four jets respectively after ordering them according to their p_T . While generating these distributions, we impose the following cuts on the p_T of leptons and jets, rest of the cuts remain unchanged,

$$p_T(\ell) > 10 \text{ GeV}, \quad p_T^{\text{jets}} > 15 \text{ GeV} . \quad (4.19)$$

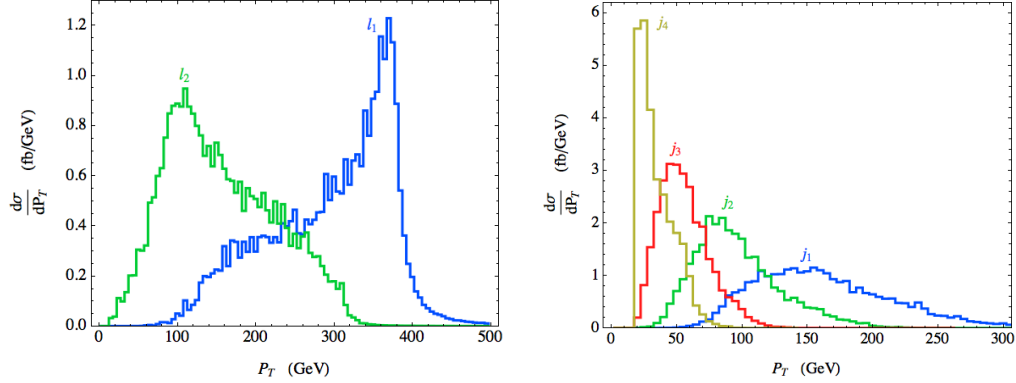


Figure 11. p_T distributions of two leptons (left-panel) and all four jets (right-panel) in the process $pp \rightarrow \mu^\pm e^\pm b \bar{b} j j$ at $\sqrt{s} = 14$ TeV. The leptons and jets are ordered according to their p_T hardness ($p_T(\ell_1) > p_T(\ell_2)$) and ($p_T(j_1) > p_T(j_2) > p_T(j_3) > p_T(j_4)$). The other model parameters are same as in Fig.8.

We take the same set of mass parameters as in the previous subsection. In this case too, the leading lepton comes from the two body decay $W_R \rightarrow \ell_1 + \nu_\mu^c$. On the other hand, the leading jet j_1 mainly comes from the two body decay of the smuon, while the second hardest jet is produced from the top quark decay. From the nature of the p_T spectrum of leptons and jets as shown in Fig. 11, we can justify our choice of p_T cuts (Eqs. (4.17) and (4.18)) used in this analysis.

In Fig. 12 we show the signal cross section (after all cuts on final state leptons and jets as mentioned above) for this channel as a function of the smuon mass at the LHC for 7 TeV, 10 TeV and 14 TeV energies. In each panel, three curves from top to bottom correspond to $M_{W_R} = 1$ TeV, 1.5 TeV and 2 TeV respectively. $M_{\nu_\mu^c}$ is kept fixed at 500 GeV and $g\theta_{eW} = 0.2$, the same as in Fig. 9. Comments on the cross sections are in order.

- In this case, since we look for $\tilde{\mu}^+ \rightarrow t \bar{b}$, we focus on the smuon mass above the top quark threshold, as is displayed in all three panels of Fig. 12. As the smuon mass increases, the leptons and jets originating from the cascade decay of smuon tend to appear with larger ΔR between each other, satisfying the isolation criteria shown in Eq. (4.12).
- The signal cross section begins to drop for heavier smuon mass (≥ 350 GeV) irrespective of M_{W_R} and choice of the LHC energy. This is mainly due to the branching ratio suppression of the $\tilde{\mu}^+ \rightarrow t \bar{b}$ decay mode, as can be seen in the right panel of Fig. 7. Secondly, there is also the phase space suppression when $M_{\tilde{\mu}}$ becomes close to right-handed neutrino mass $M_{\nu_\mu^c}$.
- In Table 5, we show the range of signal cross sections for different values of $M_{\tilde{\mu}}$ at the LHC with $\sqrt{s} = 7, 10, 14$ TeV and $M_{W_R} = 1, 1.5, 2$ TeV, respectively. The other parameters are taken as $M_{\nu_\mu^c} = 500$ GeV and $g\theta_{eW} = 0.2$. We quote the minimum and

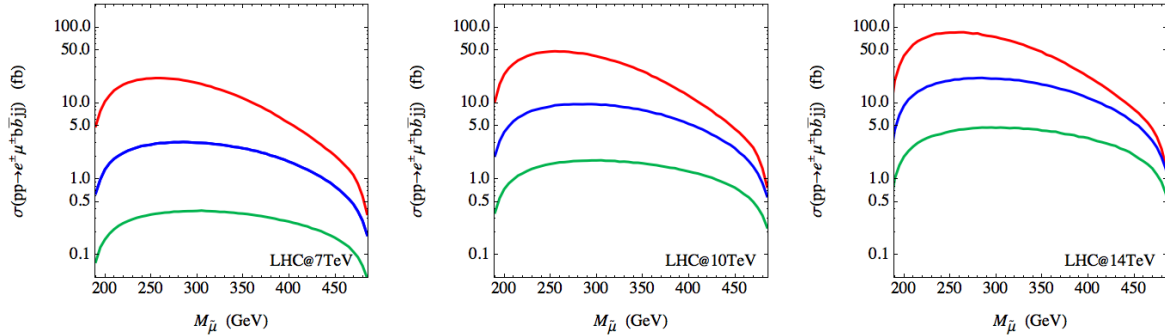


Figure 12. Signal cross sections $\sigma(pp \rightarrow \mu^- e^- b \bar{b} j j)$ (after all cuts as mentioned in the text) as a function of smuon mass at the LHC with $\sqrt{s} = 7$ TeV, 10 TeV and 14 TeV. Three curves from top to bottom in each panel correspond to $M_{W_R} = 1$ TeV, 1.5 TeV and 2 TeV respectively. $M_{\nu_\mu^c}$ is kept fixed at 500 GeV.

maximum values of the signal rate. For all three choices of M_{W_R} and \sqrt{s} the smallest cross section always correspond to the value of $M_{\tilde{\mu}}$ which is close to $M_{\nu_\mu^c}$, while the largest cross section correspond to $M_{\tilde{\mu}}$ lying between 260 – 300 GeV. The signal gets enhanced by more than factor of 2 as the LHC energy increases from 7 TeV to 10 TeV, and by another factor of 2–3 up to 14 TeV.

Mass reconstruction: We now discuss the mass reconstruction strategy of all three heavy particles from the final state charged leptons and jets. From the sample of four jets, the hadronically decaying SM W -boson is reconstructed from pair jets whose invariant mass (m_{jj}) is closest to M_W . The top quark is then reconstructed from the reconstructed W and one of the two remaining jets. We select the one which gives a invariant mass closest to M_t . The smuon mass is reconstructed from this M_t and with the last jet $M_{\tilde{\mu}} \equiv m_{tj}$. Next, we attempt to reconstruct the right-handed neutrino mass by combining with one of the two leptons ℓ_1 or ℓ_2 . In this case, we are facing the combinatorical background with two choices $m_{tj\ell_1}$, $m_{tj\ell_2}$. Finally, the W_R -boson mass can be reconstructed by combining all four jets and two charged leptons. We will not explicitly show the reconstruction figure here, which looks very similar to Fig. 10.

SM background: In this case, the standard model process which can mimic our signal is

$$pp \rightarrow t\bar{t}W^\pm \rightarrow b\bar{b}W^+W^-W^\pm \rightarrow jjb\bar{b}\ell^\pm\ell'^\pm, \quad (4.20)$$

where $\ell, \ell' = e, \mu$. In our analysis, we do not impose the requirement of b tagging, since the standard model background also contains b -jets, and b tagging would not improve the signal significance considerably. The standard model background cross sections from $pp \rightarrow t\bar{t}W^\pm$ process is shown in Table. 6, at different LHC energies. We expect this rate would further go down significantly (by several orders of magnitude) once we impose our selection criteria on the final state leptons and jets.

M_{W_R}	7 TeV	10 TeV	14 TeV
1 TeV	0.3–21.22	0.78–47.9	1.4–85
1.5 TeV	0.18–3.04	0.58–9.6	1.3–21.32
2 TeV	0.05–0.38	0.22–1.75	0.62–4.73

Table 5. The $pp \rightarrow \mu^\pm e^\pm b\bar{b}jj$ signal cross sections (in fb) at the LHC for $\sqrt{s} = 7, 10, 14$ TeV and $M_{W_R} = 1, 1.5, 2$ TeV, respectively. The other parameters are taken as $M_{\nu_\mu^c} = 500$ GeV and $g\theta_{eW} = 0.2$. Here we quote the minimum and maximum values of the signal rate and the corresponding smuon masses are shown in the text.

\sqrt{s}	$\sigma_{t\bar{t}W^\pm}$ (fb)	$\sigma_{\text{bkg}}^{\ell^\pm\ell^\pm}$ (fb)
7 TeV	99	1.32
10 TeV	206	2.77
14 TeV	377	5.05

Table 6. The dominant SM background $pp \rightarrow t\bar{t}W^\pm$ that could mimic our signal. $\sigma_{t\bar{t}W^\pm}$ correspond to the production cross-section of $t\bar{t}W^\pm$ and $\sigma_{\text{bkg}}^{\ell^\pm\ell^\pm}$ represents cross-section for $b\bar{b}jj\mu^\pm e^\pm$ final state before any cuts.

We also comment on the other standard model background $pp \rightarrow b\bar{b}jj$, which has a huge cross section $\sim 10^5$ pb after basic cuts. Taking into account of the oscillation of $b\bar{b}$ to get same-sign $e^\pm\mu^\pm P_{\ell^\pm\ell^\pm}^{b\bar{b}}$ will reduce it down to the order of ~ 1 pb. The cuts on missing energy and the hardest lepton and jet will further reduce the cross section. Moreover, in this case, highly energetic b -jet will produce charged leptons which will be very close to the associated c -jet, as a result of this, lepton-jet isolation criteria will play a decisive role in reducing this background further. Therefore, we conclude that this background will be also under control. The remaining backgrounds $pp \rightarrow W^\pm W^\pm W^\mp Z^0$, $pp \rightarrow W^\pm W^\pm W^\mp h$ and $pp \rightarrow jjjjW^\pm W^\pm$ are much smaller [36].

5 Some Generic Low-energy Constraints

5.1 Neutrinoless double beta decay

In this model, there are several new contributions to neutrinoless double beta decay in addition to the usual light neutrino contribution. The contribution from the RH neutrino exchange as in the non-SUSYLR models was already discussed [37].

In our model, there are two new contributions arising from the $e^c - \tilde{W}_R$ mixing. The first one is given in left panel of Fig. 13 below. Its contribution to the effective neutrino mass is given by

$$m_\nu^{0\nu\beta\beta} \approx \theta_{eW}^2 \left(\frac{M_{W_L}}{M_{W_R}} \right)^4 \frac{p_F^2}{m_{\tilde{W}_R}}, \quad (5.1)$$

where $p_F \approx 50 - 100 \text{ MeV}$ is the typical momentum transfer in this process. For $\theta_{eW} \sim \mathcal{O}(1)$, it is of same order as the RH neutrino contributions to this process in non-supersymmetric case.

The second contribution is given in the right panel of Fig. 13 and the corresponding effective neutrino mass is

$$m_\nu^{0\nu\beta\beta} \approx \theta_{eW}^2 \left(\frac{\alpha_s}{\alpha} \right) \left(\frac{M_{W_L}}{m_{\tilde{d}^c}} \right)^4 \frac{p_F^2}{m_{\tilde{g}}}. \quad (5.2)$$

Note that for this to be consistent with the current limits on the neutrinoless double beta decay amplitude, we must have $M_{\tilde{d}^c}, M_{\tilde{G}} \geq 1 \text{ TeV}$ for $g\theta_{eW} \sim 0.2$ [15]. This however does not constrain the slepton masses which could still be in the 100 GeV range. Unlike the conventional light neutrino mass and explicit R-parity violating contributions, these new contributions lead to RH polarization for the electron produced in the decay.

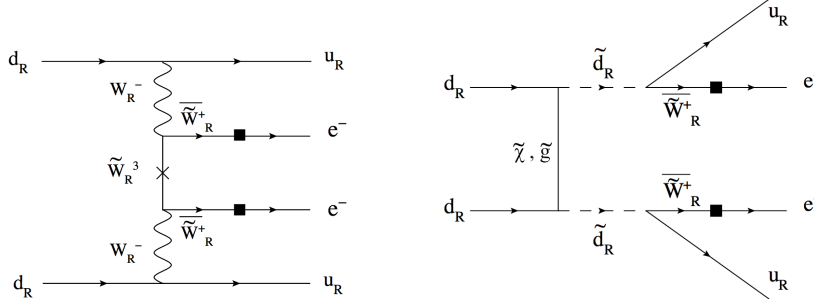


Figure 13. New contribution to neutrinoless double beta decay due to $\tilde{W}_R^+ - e^c$ mixing.

5.2 $\pi^0 \rightarrow e^+e^-$ decay

This new R-parity violating interaction also has interesting consequences for rare leptonic decays neutral pion and Kaon decays. We see from Eq. (2.5) that via t-channel \tilde{u}^c exchange this leads to the process $\pi^0 \rightarrow e^+e^-$ with an amplitude given by $A \simeq g^2\theta_{eW}^2/M_{\tilde{u}^c}^2$. The current PDG bound [38] on this process is $\text{Br}(\pi^0 \rightarrow e^+e^-) \leq 6 \times 10^{-8}$. Using the bounds from neutrinoless double beta decay, we predict that in our model we have $\text{Br}(\pi^0 \rightarrow e^+e^-) \leq 10^{-8}$. Note that if there is mixing in the right-handed charged current of the same order as the CKM mixings, then we would predict for the $K \rightarrow e^+e^-$ branching ratio at the level about 25 times smaller than corresponding pion decay. This is about 3 times smaller than the current PDG quoted bound. In the LHC search described above, we already restrict ourselves to this allowed parameter range.

6 Conclusion

In summary, we have studied the phenomenology of a class of minimal SUSYLR models with *dynamical R-parity breaking*, i.e., R-parity must necessarily break in order for parity and gauge

symmetry breaking to occur. This induces a new class of R-parity violating interactions due to the mixing between e^c and \widetilde{W}_R^+ , which are not present in the usual MSSM with explicit or spontaneous R-parity violation. These interactions lead to a new contribution to neutrinoless double beta decay which restricts the squark/gluino masses to be in the TeV range. The model has its characteristic signature at LHC which consists of final states of type $e^+e^-\mu^\pm\mu^\pm jj$ or $\mu^\pm e^\pm b\bar{b}jj$ for smuon as the NLSP. We estimate the background for this process and find that for M_{W_R} not far above a TeV, the model should be testable once LHC reaches its full energy and luminosity. Incidentally, in this model there is also an upper limit on the mass of the right-handed W_R boson in the low TeV range for symmetry breaking to occur. A large part of the mass range could be accessible even in the early running at the LHC.

Acknowledgments

We would like to thank K.S. Babu, B. Bajc, S. Biswas, I. Gogoladze, T. Han, X. Ji, G. Senjanović, S. Spinner and J. Zupan for fruitful discussions. The work of S.L.C. is partially supported by the US DOE grant DE-FG02-93ER-40762. D.K.G. acknowledges the hospitality provided by the ICTP High Energy Group, Trieste, Italy and the Regional Centre for Accelerator-based Particle Physics (RECAPP), Harish Chandra Research Institute, Allahabad, India where part of this work was done. D.K.G. also acknowledges partial support from the Department of Science and Technology, India under the grant SR/S2/HEP-12/2006. The work of R.N.M. is supported by the NSF grant PHY-0968854. The work of Y.Z. is partially supported by the EU FP6 Marie Curie Research and Training Network UniverseNet (MRTN-CT-2006-035863).

A Fully parity symmetric version

In this appendix, we consider the full parity symmetric version of the model. We now keep the Δ and $\bar{\Delta}$ multiplets in our model of Table 1. The Yukawa superpotential is given for this case by the same expression as Eq. (3.1) with two additional terms: $L^T \tau_2 \Delta L$ and $\mu_\Delta \text{Tr} \Delta \bar{\Delta}$.

The full potential that is parity symmetric is given below:

$$\begin{aligned}
V_{\text{soft}} = & m_{\tilde{Q}}^2 \left(\tilde{Q}^\dagger \tilde{Q} + \tilde{Q}^{c\dagger} \tilde{Q}^c \right) + m_{\tilde{L}}^2 \left(\tilde{L}^\dagger \tilde{L} + \tilde{L}^{c\dagger} \tilde{L}^c \right) \\
& + m_\Delta^2 \left[\text{Tr}(\Delta^\dagger \Delta) + \text{Tr}(\Delta^{c\dagger} \Delta^c) \right] + m_{\bar{\Delta}}^2 \left[\text{Tr}(\bar{\Delta}^\dagger \bar{\Delta}) + \text{Tr}(\bar{\Delta}^{c\dagger} \bar{\Delta}^c) \right] \\
& + \frac{1}{2} (M_{2L} \lambda_L^a \lambda_L^a + M_{2R} \lambda_R^a \lambda_R^a + M_1 \lambda_{BL} \lambda_{BL} + M_3 \lambda_g \lambda_g) \\
& + \tilde{Q}^T \tau_2 A_i^q \phi_i \tau_2 \tilde{Q}^c + \tilde{L}^T \tau_2 A_i^\ell \phi_i \tau_2 \tilde{L}^c + i A_f \left(\tilde{L}_L^T \tau_2 \Delta_L \tilde{L}_L + \tilde{L}_R^{cT} \tau_2 \Delta_R^c \tilde{L}_R^c \right) \\
& + B_\Phi \text{Tr} (\tau_2 \phi_a^T \tau_2 \phi_b) + B_\Delta \text{Tr} (\Delta \bar{\Delta} + \Delta^c \bar{\Delta}^c) + \text{h.c.} .
\end{aligned} \tag{A.1}$$

The D-term potential as well as the scalar potential can be found in Refs. [2, 9]. The arguments for the existence of the dynamical R-parity breaking is same as in the parity asymmetric

version discussed in sec. 2. So we do not repeat this discussion here. The only question we address here is the status of a possible parity symmetric vacuum ³ with dynamical R-parity breaking.

First, we would like to understand why the symmetry breaking in the SUSYLR model without Higgs triplets [8] is not compatible with the parity symmetry. The point is the LH and RH sneutrinos have opposite $B - L$ charges, so the D-term potential contributes a negative cross term

$$V_D \sim -\frac{1}{4}g_{BL}^2\langle\tilde{\nu}\rangle^2\langle\tilde{\nu}^c\rangle^2, \quad (\text{A.2})$$

which tends to minimize the potential in the parity conserving $\langle\tilde{\nu}\rangle = \langle\tilde{\nu}^c\rangle$. This is why the authors of Ref. [8] have to start with parity asymmetric soft mass squared for sneutrinos.

In contrast, the corresponding term in model with Higgs triplets becomes

$$V_D \sim -\frac{1}{4}g_{BL}^2\left(\langle\tilde{\nu}^c\rangle^2 - 2v_R^2 + 2\bar{v}_R^2\right)\left(\langle\tilde{\nu}\rangle^2 - 2v_L^2 + 2\bar{v}_L^2\right), \quad (\text{A.3})$$

where $\langle\Delta^0\rangle = v_L$ and $\langle\bar{\Delta}^0\rangle = \bar{v}_L$. According the D-flat condition found out in Fig. 2, each bracket is very close to vanishing. Therefore, such D-term potential does not play significant role in forcing the vacuum to preserve parity and it is still possible to start with a symmetric potential. It has been shown in [2] that if leptonic Yukawa couplings Y_ℓ satisfy the bound

$$Y_\ell^2 \geq \frac{2f^2(M_\Delta^2 - B_\Delta)}{M_\Delta^2}, \quad (\text{A.4})$$

the parity violating minimum is indeed lower than the parity conserving. By choosing M_Δ and B_Δ appropriately, we can satisfy this bound so that the parity violating and R-parity violating minimum is the global minimum.

B Explicit form of charged fermion mass matrix

In this appendix, we present the explicit form of charged fermion mass matrix in the SUSYLR model. The spontaneous R-parity violation induces a mixing between the new chargino \widetilde{W}_R , higgsino $\widetilde{\Delta}^{c+}$ and the usual electron field.

To see this explicitly, first note that parity violation at the TeV scale requires spontaneous R-parity breaking at a similar scale, i.e., $\langle\tilde{\nu}_e^c\rangle \simeq v_R \simeq \bar{v}_R$. We can write down the charged fermion mass $\frac{1}{2}\Psi^T M_{\widetilde{C}}\Psi + \text{h.c.}$, in the basis of $\Psi = [(\widetilde{W}_R^+, \widetilde{\Delta}^{c+}, e^{c+}), (\widetilde{W}_R^-, \widetilde{\Delta}^{c-}, e^-)]^T$,

$$M_{\widetilde{C}} = \begin{bmatrix} 0 & M \\ M^T & 0 \end{bmatrix}, \quad M = \begin{bmatrix} M_{1/2} & -\sqrt{2}g_R v_R & 0 \\ \sqrt{2}g_R \bar{v}_R & -\mu_\Delta & 0 \\ g_R \langle\tilde{\nu}_e^c\rangle & f \langle\nu_e^c\rangle & m_e \end{bmatrix}. \quad (\text{B.1})$$

³We thank S. Spinner for raising this point.

Following the similar arguments below Eq. (2.2), one finds the physical electron field mass term can be written as

$$\begin{aligned}\mathcal{L}_m &= -em_e(\theta_{ee}e^c + \theta_{eW}\widetilde{W}_R^+ + \theta_{e\Delta}\widetilde{\Delta}^c) + \text{h.c.} \\ &\equiv -em_e\hat{e}^c + \text{h.c.} ,\end{aligned}\tag{B.2}$$

where $\theta_{ee}, \theta_{eW}, \theta_{e\Delta}$ are order 1 mixing parameters.

In this model, the role played by $\Delta^c, \bar{\Delta}^c$ Higgses is to give mass to the RH neutrinos. Meanwhile, their superpartners enter in the above mixing matrix, but it does not change the generic prediction of large $e^c-\widetilde{W}_R^+$ mixing.

References

- [1] R. N. Mohapatra, Phys. Rev. D **34**, 3457 (1986); S. P. Martin, Phys. Rev. D **46**, 2769 (1992).
- [2] R. Kuchimanchi and R. N. Mohapatra, Phys. Rev. D **48**, 4352 (1993).
- [3] K. S. Babu and R. N. Mohapatra, Phys. Lett. B **668**, 404 (2008) [arXiv:0807.0481 [hep-ph]];
- [4] R. N. Mohapatra, Phys. Rev. Lett. **56**, 561-563 (1986).
- [5] V. Barger, P. Fileviez Perez and S. Spinner, Phys. Rev. Lett. **102**, 181802 (2009) [arXiv:0812.3661 [hep-ph]].
- [6] R. Kuchimanchi and R. N. Mohapatra, Phys. Rev. Lett. **75**, 3989 (1995).
- [7] M. J. Hayashi, A. Murayama, Phys. Lett. **B153**, 251 (1985).
- [8] P. Fileviez Perez and S. Spinner, Phys. Lett. B **673**, 251 (2009) [arXiv:0811.3424 [hep-ph]].
- [9] X. Ji, R. N. Mohapatra, S. Nussinov and Y. Zhang, Phys. Rev. D **78**, 075032 (2008) [arXiv:0808.1904 [hep-ph]].
- [10] A. Ibarra and D. Tran, JCAP **0807**, 002 (2008) [arXiv:0804.4596 [astro-ph]]; K. Ishiwata, S. Matsumoto and T. Moroi, Phys. Rev. D **78**, 063505 (2008) [arXiv:0805.1133 [hep-ph]]; S. L. Chen, R. N. Mohapatra, S. Nussinov and Y. Zhang, Phys. Lett. B **677**, 311 (2009) [arXiv:0903.2562 [hep-ph]]; W. Buchmuller, A. Ibarra, T. Shindou, F. Takayama and D. Tran, JCAP **0909**, 021 (2009) [arXiv:0906.1187 [hep-ph]]; A. Ibarra, D. Tran and C. Weniger, JCAP **1001**, 009 (2010) [arXiv:0906.1571 [hep-ph]]; B. Bajc, T. Enkhbat, D. K. Ghosh, G. Senjanović and Y. Zhang, JHEP **1005**, 048 (2010) [arXiv:1002.3631 [hep-ph]].
- [11] For some early studies concerning the Higgs/Higgsino sector of SUSYLR model, see K. Huitu, M. Raidal and J. Maalampi, arXiv:hep-ph/9501255; K. Huitu and J. Maalampi, Phys. Lett. B **344**, 217 (1995); K. Huitu, J. Maalampi and M. Raidal, Nucl. Phys. B **420**, 449 (1994) and references therein.
- [12] C. S. Aulakh and R. N. Mohapatra, Phys. Lett. B **119**, 136 (1982); G. G. Ross and J. W. F. Valle, Phys. Lett. B **151**, 375 (1985).
- [13] A. Masiero and J. W. F. Valle, Phys. Lett. B **251**, 273 (1990).
- [14] M. Arai, K. Huitu, S. K. Rai and K. Rao, JHEP **1008**, 082 (2010).
- [15] M. Hirsch, H. V. Klapdor-Kleingrothaus and S. G. Kovalenko, Phys. Rev. Lett. **75**, 17 (1995).

- [16] For a discussion on the constraints on R-parity breaking couplings from Z-pole observables, see Section 6.3.2 of Ref. [22].
- [17] J. Schmidt, C. Weniger and T. T. Yanagida, arXiv:1008.0398 [hep-ph].
- [18] S. Bobrovskiy, W. Buchmuller, J. Hajer and J. Schmidt, JHEP **1010**, 061 (2010).
- [19] It has been pointed out in C. S. Aulakh, A. Melfo, G. Senjanović, Phys. Rev. **D57**, 4174-4178 (1998), [hep-ph/9707256] that the gauge symmetry can be broken without breaking R-parity in the presence of higher dimensional operators. This, however, will push the $SU(2)_R$ breaking to high scale $\sim 10^{10-12}$ GeV, where the W_R gauge boson is not accessible at the LHC. We do not consider this possibility here.
- [20] Y. Zhang, H. An and X. d. Ji, Phys. Rev. D **78**, 035006 (2008) [arXiv:0710.1454 [hep-ph]].
- [21] D. Guadagnoli and R. N. Mohapatra, arXiv:1008.1074 [hep-ph].
- [22] R. Barbier *et al.*, Phys. Rept. **420**, 1 (2005) [arXiv:hep-ph/0406039];
- [23] H. K. Dreiner and G. G. Ross, Nucl. Phys. B **365**, 597 (1991).
- [24] D. K. Ghosh, G. Senjanović and Y. Zhang, arXiv:1010.3968 [hep-ph].
- [25] Y. Zhang, H. An, X. Ji and R. N. Mohapatra, Phys. Rev. **D76**, 091301 (2007). [arXiv:0704.1662 [hep-ph]]; Nucl. Phys. **B802**, 247-279 (2008). [arXiv:0712.4218 [hep-ph]]; A. Maiezza, M. Nemevšek, F. Nesti and Goran Senjanović, Phys. Rev. **D82**, 055022 (2010). [arXiv:1005.5160 [hep-ph]].
- [26] V. D. Barger, G. F. Giudice and T. Han, Phys. Rev. D **40**, 2987 (1989); G. Bhattacharyya, Nucl. Phys. Proc. Suppl. **52A**, 83 (1997) [arXiv:hep-ph/9608415]; H. K. Dreiner, arXiv:hep-ph/9707435. .
- [27] B. Allanach *et al.* [R parity Working Group Collaboration], arXiv:hep-ph/9906224; H. K. Dreiner and S. Grab, Phys. Lett. B **679**, 45 (2009) [arXiv:0811.0200 [hep-ph]]; G. Moreau, E. Perez and G. Polesello, Nucl. Phys. B **604**, 3 (2001) [arXiv:hep-ph/0003012].
- [28] F. de Campos, O. J. P. Eboli, M. B. Magro, W. Porod, D. Restrepo, M. Hirsch and J. W. F. Valle, JHEP **0805**, 048 (2008) [arXiv:0712.2156 [hep-ph]]; A. Bartl, W. Porod, F. de Campos, M. A. Garcia-Jareno, M. B. Magro, J. W. F. Valle and W. Majerotto, Nucl. Phys. B **502**, 19 (1997) [arXiv:hep-ph/9612436]; M. C. Gonzalez-Garcia, J. C. Romao and J. W. F. Valle, Nucl. Phys. B **391**, 100 (1993).
- [29] H. Baer and X. Tata, “Weak scale supersymmetry: From superfields to scattering events,” *Cambridge, UK: Univ. Pr. (2006) 537 p.*
- [30] W. Y. Keung and G. Senjanović, Phys. Rev. Lett. **50**, 1427 (1983).
- [31] S. N. Gninenko, M. M. Kirsanov, N. V. Krasnikov and V. A. Matveev, Phys. Atom. Nucl. **70**, 441 (2007).
- [32] T. Stelzer and W. F. Long, *Automatic generation of tree level helicity amplitudes, Comput. Phys. Commun.* **81**,357 (1994).
- [33] A. Pukhov, arXiv: hep-ph/0412191.
- [34] J. Pumplin, D. R. Stump, J. Huston, H. L. Lai, P. Nadolsky and W. K. Tung, JHEP **0207**, 012 (2002); D. Stump, J. Huston, J. Pumplin, W. K. Tung, H. L. Lai, S. Kuhlmann and

- J. F. Owens, JHEP **0310**, 046 (2003); T. Sjostrand, S. Mrenna and P. Skands, JHEP **0605**, 026 (2006).
- [35] F. del Aguila, J. A. Aguilar-Saavedra and R. Pittau, JHEP **0710**, 047 (2007) [arXiv:hep-ph/0703261].
- [36] F. del Aguila and J. A. Aguilar-Saavedra, Nucl. Phys. B **813**, 22 (2009) [arXiv:0808.2468 [hep-ph]]; P. Fileviez Perez, T. Han, G. y. Huang, T. Li and K. Wang, Phys. Rev. D **78**, 015018 (2008) [arXiv:0805.3536 [hep-ph]] and references therein.
- [37] R. N. Mohapatra, G. Senjanović, Phys. Rev. **D23**, 165 (1981); R. N. Mohapatra, Phys. Rev. D **34**, 909 (1986); M. Hirsch, H. V. Klapdor-Kleingrothaus and O. Panella, Phys. Lett. B **374**, 7 (1996); A. Ali, A. V. Borisov and D. V. Zhuridov, angular correlation,” Phys. Rev. D **76**, 093009 (2007).
- [38] K. Nakamura *et al*, (Particle Data Group), J. Phys. G **37**, 075021 (2010).